2011

CT PERFUSION INVESTIGATION OF HEPATIC HEMODYNAMICS IN A RODENT MODEL OF LIVER CIRRHOSIS

Mark Dekaban

CT PERFUSION INVESTIGATION OF HEPATIC HEMODYNAMICS IN A RODENT MODEL OF LIVER CIRRHOSIS

(Spine Title: CT Perfusion Investigation of Hepatic Hemodynamics)
(Thesis Format: Integrated-Article)

by

Mark Dekaban

Graduate Program in Medical Biophysics

A thesis submitted in partial fulfillment
of the requirements for the degree of
Master of Science

The School of Graduate and Postdoctoral Studies
The University of Western Ontario
London, Ontario, Canada

THE UNIVERSITY OF WESTERN ONTARIO
SCHOOL OF GRADUATE AND POSTDOCTORAL STUDIES

CERTIFICATE OF EXAMINATION

Supervisor	Examiners
Dr. Ting-Yim Lee	Dr. Dwayne N. Jackson
Supervisory Committee	Dr. Abbas Samani
Dr. Daniel Goldman	Dr. Michael Lock
Dr. Eugene Wong	

The thesis by

Mark Dekaban

entitled:

CT PERFUSION INVESTIGATION OF HEPATIC HEMODYNAMICS IN A RODENT MODEL OF LIVER CIRRHOSIS

is accepted in partial fulfilment of the
requirements for the degree of
Master of Science

Date_____

_____
Chair of the Thesis Examination Board

ABSTRACT

This thesis aims to evaluate the utility of dynamic contrast enhanced computed tomography (DCE-CT) imaging in conjunction with kinetic analysis (CT Perfusion) for the investigation of fibrotic liver disease. Monte Carlo simulations and sensitivity analysis of the kinetic model were used to characterize the bias, variance and covariance of perfusion parameters calculated with CT Perfusion. DCE-CT scans were performed on rats treated with carbon tetrachloride (CCl_4) for 8 weeks to induce liver fibrosis, as well as sham injected control rats. Perfusion parameters were then derived from the DCE-CT scans using CT Perfusion. CCl_4 treated rats showed significant changes in total hepatic blood flow, arterial hepatic blood flow, blood volume, and arterial fraction of blood flow. Histological samples were collected at various stages of treatment and stained with methyl blue. Digital image analysis was used to quantify fibrosis content of stained tissue. A strong correlation was found between fibrosis content and arterial fraction of blood flow ($r=.82$ $p<.00001$).

Keywords: Dynamic Contrast Enhance Computed Tomography, DCE-CT, CT Perfusion, Hepatic perfusion, Liver disease, Hepatic fibrosis, Cirrhosis, Hepatic blood flow

ACKNOWLEGEMENTS

My supervisor, Dr. Ting-Yim Lee, has provided me with guidance, sound advice, and a motivating example that has been invaluable to the completion of this thesis. To him, I offer my gratitude and deepest respect.

Special thanks goes to Jennifer Hadway, Lise Desjardins and Anne Leaist for their outstanding efforts and assistance with experiments and administrative tasks. Their friendship as much as their technical expertise has made this work possible.

Finally, I would like to thank my fellow group members of the Lee lab. Their comments and feedback have been of great assistance. In particular Dr. Errol Stewart and Dr. Xiaogang Chen, whose continued advice and technical assistance were invaluable.

To each of the above, I extend my deepest appreciation.

TABLE OF CONTENTS

Page

List of Tables

List of Figures

List of Appendices

LIST OF ABBREVIATIONS

α	aterial fraction of blood flow
AHBF	arterial hepatic blood flow
ALT	alanine transaminase
ANOVA	analysis of variance
AST	aspartate transaminase
AUROC	area under receiver operating characteristic curve
BMI	body mass index
$C_a(t)$	arterial enhancement curve
$C_{pv}(t)$	portal venous enhancement curve
CCl_4	carbon tetrachloride
COV	covariance
CT	computed tomography
DCE-CT	dynamic contrast enhanced computer tomography
DCE-MR	dynamic contrast enhanced magnetic resonance
E	extraction fraction
ELF	enhanced liver fibrosis
EVS	extravascular space
$\bar{F}$	Fisher information matrix
F_a	hepatic arterial blood flow
F_{pv}	hepatic portal venous blood flow
F_T	total hepatic blood flow
HABR	hepatic arterial buffer response
HBV	hepatitis B virus
HCC	hepatocellular carcinoma
HCV	hepatitis C virus
HDV	hepatitis D virus
HIV	human immunodeficiency virus
HSC	hepatic stellate cell
HVPG	hepatic venous pressure gradient
IRF	impulse residue function
IVS	intravascular space
k	rate constant for the back flux of contrast from the extravascular to the intravascular space
LSEC	liver sinusoidal endothelial cell
LSM	liver stiffness measurement
MR	magnetic resonance
MRE	magnetic resonance elastography
MRI	magnetic resonance imaging
NO	nitric oxide
PDGF	platelet derived growth factor
PET	positron emission tomography
PHBF	portal hepatic blood flow
PPAC	percent positive area of stained collagen

PS	permeability surface area product
PW	perfusion weighted
Q(t)	tissue enhancement curve
R(t)	impulse residue function
ROI	region of interest
SF	sensitivity function
T_c	vascular mean transit time
T_0	time delay between start of arterial and tissue enhancement curves
TDC	time density curve
US	ultrasound
V_b	blood volume
V_e	distribution volume of contrast in the extravascular space
VEGF	vascular endothelial growth factor

CHAPTER 1

INTRODUCTION AND BACKGROUND TO HEPATIC FIBROSIS AND CHIRROSIS

1.1 INTRODUCTION TO THE LIVER

The liver is a vital organ that has many functions within the body. The primary functions include detoxification synthesis and production of substrates necessary for metabolism of lipids and carbohydrates. Situated in the upper abdomen behind the right ribcage and below the diaphragm, the liver blood flow is supplied by two sources (See Figure 1.1). The portal vein supplies blood from the spleen, gut and other mesentery, and accounts for approximately 75% of total liver blood flow. The remaining 25% of liver blood flow is supplied from the hepatic artery [1]. Owing to the higher oxygen content of arterial blood, oxygen delivery to the liver is about equally derived from the portal vein and hepatic artery.

The liver plays an essential role in metabolism and has numerous roles in the body, including glycogen storage, decomposition of red blood cells, plasma protein synthesis, hormone production, and detoxification. Unlike other organs, the liver benefits from a substantial regenerative capability. If as much as fifty percent of its overall mass is surgically removed or damaged by intoxication, the liver is still capable of complete regeneration [2]. This regenerative ability makes the liver extremely resilient to toxins and disease, however, chronic liver injury over prolonged periods will result in the replacement of normal healthy liver tissue with non-functioning scar tissue (fibrosis) and reduced liver function. This scarring disrupts the

normal liver architecture, leading to a resistance to blood flow through the liver. When the scarring progresses far enough that it encapsulates regenerating nodules of liver parenchyma, the condition is referred to as cirrhosis. Cirrhosis is a potentially life-threatening condition with serious complications. The following section describes causes of cirrhosis and its complications

1.1.1 Liver Disease

The Canadian Liver Foundation estimates that 3 million Canadians, including men, women and children, are currently living with some form of liver diseases. The most common causes of liver disease in Canada are listed below:

- Viral infections such as hepatitis B, C and D virus (HBV, HCV, HDV)
- Non-alcoholic fatty liver disease
- Chronic alcoholism
- Genetic disorders such as hemochromatosis and Wilson disease
- Autoimmune disorders such as primary biliary cirrhosis or primary sclerosing cholangitis

Treatment of liver disease can be labor intensive and costly [3]. It is estimated that the annual cost to treat HCV infected intravenous drugs users alone, in Canada, is approximately $176,000,000. [4]

No matter the etiology, the liver has a common innate wound healing response to chronic liver injury characterized by fibrosis of the liver. If the cause of the insult cannot be removed, fibrosis will progress to cirrhosis and eventually liver failure and death.

Normally blood flow from the intestines and spleen is pumped through the portal vein. The altered vasculature of a cirrhotic liver presents a large resistance to blood flow. This resistance is measured as the pressure gradient between and the portal vein and the inferior vena cava, also known as the hepatic venous pressure gradient (HVPG). In a normal liver the HVPG is less than 5mmHg. A HVPG greater than 10mmHg is known as portal hypertension [5]. The major complications of portal hypertension are ascites, gastrointestinal hemorrhage and renal dysfunction.

Ascites is the accumulation of fluid in the peritoneal cavity, driven by increased capillary hydrostatic pressure within the splanchnic bed as a result of portal hypertension. Ascites carries a risk of spontaneous bacterial peritonitis and sepsis. Diuretics can be used to control the accumulation of fluids but as liver disease progresses this becomes more difficult[6]. Ascites and the abnormal handling of sodium in combination with altered systemic circulation leads to hepatorenal disease [6]. Liver transplant is the only long-term solution to hepatorenal disease, after which kidney function returns to normal or near normal levels. [7]

When the HVPG is greater than 10mmHg, blood flow though the hepatic portal venous system is redirected from the liver into areas with lower venous pressures. This means that collateral circulation develops in the lower esophagus, abdominal wall, stomach and rectum. The small, thin walled vessels become distended and are at risk of rupture, causing the patient to bleed internally.

Portal hypertension and its complications are the leading cause of morbidity and mortality in patients with cirrhosis. [8]

Hepatocellular carcinoma (HCC) is also a common complication for patients with liver disease. It has been estimated that 80% of all HCC occurs in a cirrhotic background[9]. The annual risk of developing HCC for patients with HCV infection has been estimated to be 3-8%[9].

1.2 MICROSTRUCTURE OF THE LIVER

The hepatocyte is the primary parenchymal cell of the liver, making up 80% of the total hepatic cell population. They are arranged in unicellular plates, sometimes referred to as Remak's plates. These plates branch and anastamose with each other forming a maze like arrangement of partitions. Between the plates of hepatocytes are the liver sinusoids. Liver sinusoids can be regarded as unique capillaries. Unlike typical capillaries, the sinusoids have a discontinuous endothelial layer and lack a basement membrane [10]. This endothelial layer is made up of specialized liver sinusoidal endothelial cells (LSEC), which have groups of fenestrations (pores) measuring 150–175 nm in diameter [11]. These fenestrations act as a dynamic filter for fluids, solutes and particles, allowing only particles smaller than the fenestrae to reach the parenchymal cell [10]. Between the endothelial layer and the hepatocytes is the space of Disse. This space is primarily filled with hepatocyte microvilli as can be seen in Figure 1.2, which allows proteins and other components of plasma to be absorbed by the hepatocytes. The hepatic stellate cell (HSC), also known as the Ito cell, lipocyte or fat-storing cells, resides within the space of Disse. The HSC is the major cell type involved in the pathogenesis of liver fibrosis, as is discussed in further detail in section 1.3. Kupffer cells are resident liver macrophages within the sinusoidal

space where they can phagocytose and destroy foreign material such as bacteria.

Blood flow at the microscopic level originates at the portal triads. The portal triads consist of an arrangement of branches from the hepatic artery, portal vein, and bile duct, as well as lymphatic vessels. Blood supplied by the hepatic artery and portal vein passes through the sinusoids and empties into the central veins, which then coalesce into the hepatic veins. Figure 1.3 shows a representation of the microvascular structure of the liver.

1.3 HEPATIC FIBROSIS AND VASCULAR REMODELING

A great deal of progress has recently been made in understanding the pathogenesis of hepatic fibrosis. Fibrosis, or scarring of the liver, is a wound-healing response that engages a range of cell types and mediators to encapsulate injury. Although acute injury will activate mechanisms of fibrogenesis, the sustained signals associated with chronic liver disease caused by infection, drugs, metabolic disorders, or immune attack are required for significant fibrosis to accumulate. Under certain circumstances a normal, or mildly fibrotic liver may rapidly progress to cirrhosis over several weeks or months. For example, patients with HCV receiving immunosuppressant drugs after liver transplant can have high viral load resulting in a rapid progression to cirrhosis [12]. A similar situation exists in patients with human immunodeficiency virus (HIV)/HCV co-infection [13].

The hepatic stellate cell is the primary cell in the liver responsible for excess collagen synthesis during hepatic fibrosis[14]. Upon injurious stimuli the HSC

undergoes 'activation' which is a complex transformation to a proliferative, contractile, myofibroblast-like cell. In reviewing the mechanisms of hepatic fibrosis, Firedman S. defined three stages of fibrosis based on the activation of stellate cells [15]. These stages are initiation, perpetuation, and resolution. Initiating stimuli include paracrine signals such as reactive oxygen species from apoptotic hepatocytes, injured cholangiocytes, macrophages, stellate cells, and inflammatory cells [16 17]. Early injury of LSECs stimulates the production of cellular fibronectin, as well as platelet derived growth factor (PDGF), which has an activating effect on stellate cells[18]. Apoptosis has also been implicated in the fibrogentic response[19]. Apoptotic proteins released from hepatocytes are fibrogenic towards cultured stellate cells[20,21].

These initial parcrine signaling pathways result in changes in gene expression and phenotype allowing the now 'activated' HSC to respond to new stimuli leading to perpetuation. The induction of type I collagen gene expression causes the HSC to become directly fibrogenic [22 23]. In addition, PDGF and it's receptor have been shown to be rapidly induced in culture and in vivo [24 25], resulting in proliferation as well as chemotaxis [26]. The expression of PDGF by LSECs along with the mitogenic effect of PDGF on HSCs results in an enhanced coverage of sinusoids by HSCs in vivo [27].

Contractility is another key feature of the activated HSC. HSC's have been demonstrated to have contractile capability both in-vivo and in-vitro [28]. This contractile capability is mediated primarily by endothelian-1 (ET-1) and inhibited by nitric oxide (NO) produced by LSECs [29 30]. During liver injury, LSEC show impaired generation of NO resulting in vasoconstriction[31].

The combination of proliferated HSCs covering the sinusoidal lumen, and their

subsequent contraction from reduced NO production in LSECs, results in a constricted sinusoidal space. This alteration in the normal vascular structure, in combination with increased deposition of collagen, contributes to increased intrahepatic sinusoidal pressure, portal hypertension, and it's subsequent complications [27 32].

The activated HSC is not simply a fibrogenic cell, it also plays an important role in vascular structural changes and angiogenesis in hepatic fibrosis. Angiogenesis is the dynamic formation of new vessels from pre-existing vessels [33,34]. Angiogenic processes occur throughout the body and are associated with tissue damage, wound healing and vascular remodeling. Thus, it should come as no surprise that angiogenesis occurs concurrently with hepatic fibrosis. Stimulation of angiogenesis during hepatic fibrosis is thought to come from several possible sources. Vascular endothelial growth factor (VEGF) is produced by hepatocytes in response to hypoxia [33 35] as well as an autocrine signaling loop within LSECs [33 36]. Activated HSCs have also been shown to express angiogenic factors such as VEGF and angiopoietin-1 [37 38]. HSCs and LSECs play a unique dual role in both fibrogenesis and angiogenesis as part of a total wound healing response. As a result anti-angiogenic drugs originally designed for cancer treatments have seen renewed interest for the treatment of hepatic fibrosis and it's complications. The inhibition of the PDGF signaling pathway by the receptor tyrosine-kinase inhibitor Imatinib was capable of reducing portal pressure in an animal model of cirrhosis [27 39]. Reduced portal pressure was primarily the result of reduced sinusoidal coverage by HSCs, thus resulting in reduced constriction of the sinusoids. Although portal pressure was reduced no reduction in fibrogenesis was

observed [27 39].

The resolution phase is still not completely understood. With the removal of the underlying cause of liver injury, activated HSCs may revert back to a quiescent state or be cleared through an apoptotic pathway [30]. Reversibility of fibrosis and cirrhosis is still a debated topic but recently there has been increasing evidence that fibrosis and cirrhosis can resolve to at least some extent [40 41 42].

A strong motivation for the use of perfusion imaging in hepatic liver disease is evident. The combination of vascular remodeling and the role of angiogenesis in the development of cirrhosis mark it as a disease with significant vascular consequences. One direct consequence of vascular changes in liver cirrhosis is portal hypertension. Portal hypertension is a major complication of liver cirrhosis representing a primary cause of death or liver transplant [5 43]. Currently the only measure of portal hypertension is the HVPG. This technique is highly invasive and impractical under normal circumstances however, it is also currently the best predictor of complications from cirrhosis and the development of HCC [43 44]. Non-invasive dynamic contrast enhanced magnetic resonance (DCE-MR) perfusion measurements have already been correlated to the HVPG in cirrhotic patients [45]. Further research into perfusion imaging techniques may provide useful non-invasive biomarkers of fibrotic liver disease. These biomarkers could be capable of predicting disease outcome and aid in patient treatment planning.

1.4 HEPATIC CIRCULATION AND BLOOD FLOW REGULATION

Roughly 25% of blood flow and 50% of oxygen is delivered to the liver from the hepatic artery. The remaining 75% of blood flow and 50% of oxygen is supplied from the portal vein. Total Hepatic blood flow is estimated to be approximately 25-30% of cardiac output. Normal changes to hepatic blood flow can result from a variety of conditions. Exercise and sleep have been shown to cause a decrease in hepatic blood flow [46], while an increase in hepatic blood flow has been observed in the postprandial state [47]. Finally, hepatic blood flow tends to decrease with increasing age [48].

Regulation of blood flow in the liver is governed through three different sites. Arterial flow is controlled by terminal hepatic arterioles, which are richly supplied in smooth muscles cells. Portal flow is dependent on the flow in the supplying organs and thus, is determined by the arterioles of these organs (eg. spleen and mesentery). Finally, liver sinusoids and terminal hepatic venules are a source of intrahepatic resistance [47]. Blood flow in the liver is influenced by both intrinsic and extrinsic mechanisms.

1.4.1 Intrinsic hepatic blood flow regulation

In autoregulation, increased arterial perfusion pressure results in hepatic artery vasoconstriction, presumably because of a myogenic response of the arteriolar smooth muscle to stretch imposed by the increased perfusion pressure [REF]. Pressure-flow autoregulation in the hepatic arterial system exists to some extent in the postprandial liver, but probably not in the fasted liver [49 50]. There is no evidence of autoregulation

in the portal venous system; instead of the nonlinear pressure-flow relationship associated with autoregulation, there exists a linear pressure-flow relationship [51].

Changes in the composition of the portal venous and systemic blood composition affect liver blood flow. These changes include arterial hypoxemia [52], systemic hypercapnia [53], and alkalosis [54]. Hepatic arterial blood flow is increased by decreased portal oxygen tension and pH [54].

A relationship between arterial and portal venous blood flow has long been known to exist. It was demonstrated that an occlusion of the portal vein results in an immediate rise in hepatic arterial blood flow [55]. This response of increased hepatic arterial blood flow in response to a decrease in portal blood flow is called the 'hepatic arterial buffer response' (HABR) [56]. Lautt et al. [57] suggested that a change in the concentration of adenosine, a vasoactive molecule, was responsible for this relationship. Adenosine is released at a constant rate in the space of Mall, which contains the hepatic arterioles and portal venules, and its concentration is regulated by washout into these vessels, principally the portal vein. Thus, a drop in portal blood flow would induce an increase in the local concentration of adenosine, which would in turn increase arterial blood flow [57]. Conversely, an increase in portal flow would increase clearance of adenosine, causing arterial vasoconstriction. As further evidence, it has been shown in the rabbit that the adenosine receptor antagonist, 8-phenyltheophylline, inhibited this response while, the adenosine uptake inhibitor, dipyridamole potentiated the HABR [58]. Although increases in hepatic arterial blood flow result only in a partial compensation for decreased portal flow, oxygen delivery is maintained, even in cirrhotic livers [59]. While portal perfusion has a large effect on

arterial blood flow, the reverse is not true. Changes in hepatic arterial flow have not been shown to cause significant changes in the portal venous flow [57].

Despite identifying adenosine as the clear regulator of the HABR, the exact cell type or site of adenosine production, as well as the specific biochemical pathway have yet to be identified. It is suggested that the adenosine involved with the HABR and autoregulation is produced at a constant rate and secreted into the space of Mall. This adenosine is most likely derived from demethylation of S-adenosylhomocysteine, a reaction that is oxygen independent and is proposed to account for basal adenosine production in the heart [60].

Although the exact site of interaction of the hepatic artery and portal vein has not been identified, it is clearly occurring at a very localized level. Lobular changes in blood flow, due to selective ligation of the portal inflow, clearly demonstrates this [61]. When portal flow to a single lobe was reduced by ligation, an increase in portal flow occured in the other lobes. The ligated lobe showed an increase in arterial blood flow while the unligated lobes showed a decrease in arterial flow. This demonstrates lobular independence of the HABR [61].

In patients with cirrhosis, the HABR is blunted [62]. A reduction in portal perfusion due to increased intrahepatic sinusoidal resistance has been observed in cirrhotic patients [63]. This sustained reduction in portal flow results in the continuous activation of the HABR [64]. Accordingly, the HABR could play a protective role in hepatic circulation by maintaining oxygenation [65].

The continuous activation of the HABR in patients with fibrotic liver disease provides a potential target for evaluating the stage of liver disease as well as the risk

of complications. The continuous, adenosine mediated, activation of the HABR has been implicated in the development of hepatorenal disease [66], which is a severe complication of liver disease that can result in death. Currently, perfusion imaging techniques are the only non-invasive way to regionally measure hemodynamic changes in the liver that are consistent with the HABR. This thesis attempts to measure hemodynamic changes in a rat model of liver fibrosis using dynamic contrast enhanced CT (DCE-CT) scanning or CT Perfusion.

1.4.2 Extrinsic hepatic blood flow regulation

Branches of the vagus, splanchnic, and sometimes phrenic nerves enter the liver mainly in association with the blood vessels and bile ducts. The sympathetic and parasympathetic nerves form an intercommunicating plexus, which terminates on arterioles and venules. Functional vagal innervation does exist in the dog and influences regional distribution within the liver by exerting effects on presinusoidal sphincters [67], rather than by affecting total liver blood flow.

Of the systemic hormones, epinephrine is the most likely to attain vasoactive concentrations physiologically. Both alpha and beta-adrenergic receptors are present in the hepatic arterial bed, whereas only alpha receptors exist in the portal vasculature [68]. Thus, epinephrine injected directly into the hepatic artery initially induces vasoconstriction via the alpha receptors, followed by vasodilation mediated by the beta receptors; the portal bed only vasoconstricts in response to intraportal epinephrine.

Glucagon causes a graded and long-lasting hepatic arterial vasodilation and can antagonize the hepatic arterial vasoconstrictor responses to a wide range of physiologic stimuli, including stress-induced sympathoadrenal outflow [69]. Angiotensin II evokes profound vasoconstriction of both hepatic arterial and portal beds, together with a significant reduction in mesenteric outflow, and this translates into a substantial reduction in total liver blood flow [70]. Vasopressin also induces marked splanchnic vasoconstriction; consequently, reduction in venous outflow into the portal system and a reduction in inflow resistance in the portal vasculature occurring after vasopressin administration make this hormone very effective in alleviating portal hypertension [71].

1.5 ANIMAL MODELS OF LIVER FIBROSIS AND CIRRHOSIS

Several experimental models of hepatic fibrosis have been developed. These include chemically induced fibrosis using hepatotoxic agents such as carbon tetrachloride (CCl_4) [72], dimethylnitrosamine [73] and thioacetamide [74], immunological damage[75], biliary fibrosis via common bile duct ligation[76], and alcoholic liver disease such as the Tsukamoto/French model in rats[77].

Carbon tetrachloride is the most commonly used toxin-based experimental model of liver fibrosis. It can be easily administered to rodents by inhalation, gastric gavage, and subcutaneous or intraperitoneal injections [77]. The trichloromethyl radical, a metabolite produced by cytochrome P450 in hepatocytes leads to lipid peroxidation and membrane damage[77], which results in acute centrilobular liver necrosis. CCl_4

models of liver fibrosis have the advantage of being well characterized with respect to the histological and biochemical changes associated with injury, inflammation, and fibrosis[77,78]. A further asset of CCl_4 models for in vivo animal studies is the ability to elicit a predictable and reproducible response. The administration of barbiturates in drinking water can enhance the activation of cytochrome p450, enhancing CCl_4 liver injury, and is a common method of hastening the development of fibrosis. With a combination of barbiturates and CCl_4 treatment, development of fibrosis can occur in as few as four weeks, and cirrhosis as early as eight weeks.

CCl_4 models do have limitations. First, there is no direct human disease counterpart[78], and second, there is a failure to progress to the development of hepatocellular carcinoma unlike the dimethylnitrosamine model of fibrosis [79]. Although depending on the requirements of the fibrosis model, lack of cancerous progression could also be viewed as an advantage.

A combination of CCl_4 and the barbiturate, phenobarbital, are used in this thesis to develop fibrosis and cirrhosis in rats. A detailed description of the methodology can be found in chapter 3.

1.6 NON-INVASIVE METHODS FOR THE INVESTIGATION OF HEPATIC FIBROSIS AND CIRRHOSIS

The current gold standard for assessing fibrosis is liver biopsy through a percutaneous, transjugular, laparoscopic, or fine-needle approach. This invasive method can be painful and carries a small but significant risk of serious

complications[80]. Further limitations come with the analysis liver biopsy samples. Histological grading is not reproducible; there are both intra- and inter-observer variability on small sized or fragmented biopsy samples[81]. Because of these limitations, biopsy is an impractical method for the regular monitoring of liver fibrosis. As new anti-fibrotic treatments are developed, there is a growing need for non-invasive methods of evaluating these treatments, as well as monitoring the progression of hepatic fibrosis in patients. The most promising methods currently under development are reviewed below.

1.6.1 Serum indices

Serum markers can be divided into direct and indirect markers of fibrosis. Direct markers are fragments of the liver matrix components produced by HSCs during the development of fibrosis, and the molecules involved in regulating the progression of fibrosis. These include hyaluronic acid, collagens IV and VI, and amino terminal fragment of procollagen III. Indirect markers of fibrosis include molecules released into the blood due to liver inflammation, such as alanine aminotransferase (ALT) and aspartate aminotransferase (AST), molecules synthesised, regulated or excreted by the liver (such as clotting factors, cholesterol and bilirubin), and processes that become deranged as liver function becomes impaired, such as insulin resistance. Both direct serum markers, and indirect serum markers have been thoroughly investigated [82 83 84 85 86]. When these markers are used individually they can reasonably diagnosis or exclude cirrhosis but lack the ability to differentiate intermediate stages of fibrosis. To increase diagnostic capability,

algorithms combining multiple serum markers, such as Fibrotest or the Enhanced Liver Fibrosis (ELF) test have been proposed to improve diagnostic accuracy. In a meta-analysis Fibrotest was able to distinguish between METAVIR stages ≦F1 vs ≧F2 or 'clinically significant' fibrosis with area under the receiver operating characteristic curve (AUROC) of .84 [87]. Currently, the ability to measure direct serum markers is not routinely available in most hospitals. Additionally, direct serum markers are not liver specific thus; they require patient specific considerations to be taken into account when interpreting the results.

1.6.2 Transient elastography

Transient elastography is performed with an ultrasound transducer probe mounted on the axis of a vibrator. A vibration transmitted from the vibrator toward the tissue induces an elastic shear wave that propagates through the tissue. The velocity of the shear wave is then measured using pulse-echo ultrasound acquisitions. The harder the tissue, the faster the shear wave propagates [88]. Transient elastography is advantageous in that it can be repeatedly performed, does not require a highly experienced operator, and has a low risk of complications. Results of several recent studies have shown that measurement of liver stiffness with transient elastography is excellent for the diagnosis of cirrhosis, but lacks sensitivity and specificity for the intermediate stages of fibrosis[89]. The reproducibility of transient elastography is also substantially reduced in patients with steatosis and increased body mass index (BMI), as well as patients with ascities. This is because ultrasonography itself has limitations for clearly visualizing the liver in such patients. [90]

1.6.3 Magnetic resonance elastography (MRE)

MRE is a promising non-invasive method for monitor the progression of liver fibrosis. MRE typically uses vibrations generated by external driver devices within the audio frequency range to induce shear waves in the liver. A signal generator triggered by and synchronized to the MR pulse sequence creates the electrical signal for these devices. A modified phase-contrast technique is used to image the propagation characteristics of the acoustic shear waves [91] [92]. The technique is easily implemented on a conventional MRI system with modest additional hardware and software. Several studies have demonstrated the excellent diagnostic capability of MRE to stage liver fibrosis [93] [94] [95], but activity of the underlying cause and steatosis seem to influence measurements [95].

While MR elastography is a promising new method for staging liver disease it does not provide vital functional information about the liver. For the evaluation of new anti-fibrotic treatments a reduction in fibrotic content and reduced liver stiffness may not necessarily indicate successful treatment. For a patient with portal hypertension, a reduction in fibrosis content and liver stiffness is not clinically relevant unless it is accompanied by hemodynamic changes that alleviate the portal hypertension. Reversal of hemodynamic changes must accompany the reduction in fibrosis content for treatment to be completely successful.

1.6.4 Dynamic contrast enhanced computed tomography (DCE-CT)

Dynamic contrast enhance computed tomography (DCE-CT) was developed in the late 1970s, with the aim of studying hemodynamics in tissue [96]. However, spatial and temporal resolutions of early hardware limited the widespread acceptance of DCE-CT. Advancements in CT scanning technology over the years has addressed these issues. The implementation of slip ring technology has increased temporal resolutions to the sub-second mark. Detector technology has also progressed, allowing DCE-CT imaging of whole organs, such as the liver, in a single study. These advancements have allowed DCE-CT to become a more competitive imaging modality, as well as to gain wider clinical acceptance. Some of the benefits of DCE-CT include its widespread availability in hospitals, its rapid scan times, with excellent spatial and temporal resolution, and its ability to image soft tissues, bone and blood vessels. Drawbacks of DCE-CT include use of contrast agents, which can impair renal function, and the exposure to carcinogenic ionizing radiation.

DCE-CT has become a valuable clinical and research tool in the study of angiogenesis and vascular changes associated with cancer and stroke diseases [97 98]. Various methods have been developed to measure hepatic perfusion *in vivo*. These include Doppler ultrasound (US) [45], dynamic contrast enhanced magnetic resonance (DCE-MR)[99] and DCE-CT [97]. Compared to Doppler US, which is capable of measuring blood flow velocity in large vessels, DCE-CT is able to measure perfusion, blood volume, mean transit time, and capillary permeability surface area product in a single study[97] In addition to this, DCE-CT can provide regional information that Doppler ultrasound can not. This set of functional parameters provides a more complete evaluation of tissue hemodynamics [97].

The use of MR as a modality for perfusion techniques seems appealing due to the lack of ionizing radiation. However, MR lacks a linear relationship between the concentration of the gadolinium-based contrast agent and MR signal intensity. This fact along with velocity-induced signal intensity changes in larger vessels has created difficulties in obtaining quantitative perfusion data with DCE-MR [100]. In contrast, the relationship between iodine concentration and x-ray attenuation during DCE-CT examination is linear.

The maximum slope method for calculating liver perfusion is a commonly used method based on the Fick Principle [100]. If F is blood flow and $C_a(t)$ is the contrast concentration at the arterial inlet and $C_v(t)$ the contrast concentration at the venous outlet then:

$$Q(T) = F \cdot \int_0^T [C_a - C_v] \cdot dt \qquad (1)$$

Where Q(t) is the contrast concentration in the tissue at time T. If T is less than the minimum transit time of the contrast agent through the capillaries, then one can assume no venous outflow and thus,

$$Q(T) = F \cdot \int_0^T C_a \cdot dt \qquad (2)$$

or,

$$\left[\frac{dQ(t)}{dt}\right]_{t=T} = F \cdot C_a(T) \qquad (3)$$

The rate of contrast accumulation in the tissue, dQ(t)/dt, will be maximal when the arterial concentration is maximal. Solving for blood flow gives,

$$F_{t=T} = \frac{\left[\frac{dQ(t)}{dt}\right]_{max}}{C_a(t)_{max}} \quad (4)$$

The ratio of the maximum rate of contrast accumulation, or maximum slope of dQ(t)/dt to the maximum arterial concentration is equal to the blood flow.

The liver however, receives blood flow from both the hepatic artery and the portal vein, which further complicates the calculation. The tissue concentration curves from each blood flow source are overlaid, because the arrival of the contrast from the portal vein arrives seconds after the contrast from the hepatic artery. To separate the two concentration curves one can use the concentration curve from the spleen. Because of the arrival time of the contrast agent through the body, one can assume that peek enhancement of the spleen occurs after the maximum rate of change of the contrast concentration in the liver tissue. Knowing this, the hepatic arterial blood flow can simply be calculated by the maximum slope of the tissue concentration curve, before peak splenic enhancement, divided by the peak hepatic arterial concentration, $C_a(t)_{max}$. Calculation of portal perfusion is more complex because the initial slope of the portal concentration curve is overlaid by the hepatic arterial concentration curve.

If one assumes that the liver and spleen show similar contrast agent dynamics during he arterial phase then the ratio of the hepatic arterial blood flow to the splenic blood flow should be equal to the ratio of their concentration curves. Hence, a model curve of pure arterial hepatic enhancement is computed by multiplying the splenic time-concentration curve by the ratio of the maximum arterial liver gradient to the maximum splenic gradient of the time-attenuation curves. This model curve is then subtracted from the original hepatic concentration curve, Q(t), resulting in a portal

venous concentration curve of the liver, $Q_{pv}(t)$, separate from its arterial component. Portal perfusion can then be calculated from $dQ_{pv}(t)/dt$ divided by the the peak of the portal venous concentration curve $C_{pv}(t)$.

The maximum slope method has two main drawbacks. First the no venous outflow assumption may not always hold true, especially in a cirrhotic liver, which can have substantial shunt formation [101]. Second the use of the splenic concentration curve to model the hepatic arterial concentration curve has not been validated.

CT Perfusion (GE healthcare) is a commercially available software package capable of analyzing DCE-CT datasets. It has been validated in the rabbit liver using radioactive microspheres as the gold standard [102], as well as in brain tumor [103] and VX2 thigh tumors[104].

With its ability to assess hemodynamics in a non-invasive fashion, DCE-CT offers a way of tracking the progression of hepatic fibrosis and cirrhosis *in vivo* [102]. This thesis attempts to evaluate the utility of DCE-CT coupled with CT Perfusion in the assessment of fibrotic liver disease. This is done using Monte Carlo simulation techniques as well as correlating CT Perfusion parameters to fibrotic content in a CCl_4 rat model of hepatic fibrosis.

DCE-CT studies were performed on rats with a clinical multi-slice CT scanner (Discovery VCT, GE Healthcare). At DCE-CT examination, an iodinated contrast agent is injected via a peripheral vein while the CT scanner is used to measure the passage of contrast through the vasculature and the uptake of contrast in the extravascular (Disse) space, followed by the subsequent washout. In the analysis of the DCE-CT data there are two fundamental underlying assumptions. The first is that

the iodinated contrast agent is uniformly distributed throughout the vascular system and the second is that the enhancement (increase in attenuation) of a particular tissue is proportional to the concentration of the contrast agent in the tissue.

A localization scan was first performed to place eight 5mm slices covering the entire rat liver. After the scan location was selected the DCE-CT scan was conducted in two phases. In the first phase, images were acquired in cine mode under breath hold by turning off the ventilator with a tube voltage and current of 120kVp and 80mA respectively and a gantry speed of one rotation per second. Images were reconstructed using the detail reconstruction filter and a temporal resolution of 0.45 seconds. Total time for the first phase cine scan was 34 seconds. In the second phase the ventilator was turned on with a breath rate of 80 breaths per minute and animals were scanned in cine mode for 1.2 second, every 10 seconds, up to a total of two minutes. This two phase scanning protocol was designed for imaging a ventilated rat under 'forced' breath hold in the first phase by turning off the ventilator and ventilated breathing in the second phase. Chapter 3 gives further detail on animal procedures as well as the registration of the second phase images.

The acquired two phase DCE-CT data were analyzed with CT Perfusion software (GE Healthcare) to derive quantitative maps of total hepatic blood flow (F_T), hepatic arterial blood flow (F_a), blood volume (V_b), mean transit time (T_c), permeability surface area product (PS), as well as the hepatic arterial fraction of blood flow α.

When a bolus of contrast agent is injected into a peripheral vein, the rate of delivery of contrast agent to the capillary network in a unit mass of tissue is

$F_T \cdot [\alpha C_a(t)+(1-\alpha)C_{pv}(t)]$, where F_T is total liver blood flow in ml/min per unit mass of liver tissue and $\alpha C_a(t)+(1-\alpha)C_{pv}(t)$ is a weighted sum of the contrast concentration over time in the hepatic artery (C_a) and portal vein (C_{pv}) with the α being the fraction of F_T that is derived from hepatic artery. If the mass of contrast in tissue (vessels plus Disse space) is linear with respect to the arterial concentration and F_T remains constant in time, then the following relationship holds true as a result of linear superimposition:

$$Q(t) = F_T \cdot \left[\alpha C_a(t) + (1-\alpha) C_{pv}(t)\right] * R(t) \qquad (5)$$

where Q(t) is the concentration of contrast in tissue over time, R(t), is the impulse residue function (IRF), and * is the convolution operator. Q(t), $C_a(t)$, and $C_{pv}(t)$ in equation (5) can be measured by dynamic CT scanning as described previously and deconvolution between these two curves then yields $F_T \cdot R(t)$, the flow-scaled impulse residue function (See Figure 1.4). R(t) describes the mass of contrast that remains in the tissue following bolus injection of a unit mass of contrast [105]. The algorithm used in CT Perfusion for the calculation of the functional parameters is based on the adiabatic approximation of the Johnson-Wilson model, a hybrid compartment and distributed parameter model with bidirectional exchange of contrast between the intravascular space and the extra vascular space [106 107]. The adiabatic approximation assumes that the tracer concentration in parenchymal tissue changes slowly relative to that in hepatic sinusoids. This assumption allows for a closed-form mathematical solution to the flow-scaled impulse residue function, $F_T \cdot R(t)$ where R(t) is defined by :

$$R(t)=\begin{cases}1 & 0\le t<T_o\\ 1.0 & T_o\le t_c\le T_o+T_c\\ Ee^{-k(t-T_o-T_c)} & t>T_o+T_c\end{cases} \quad (6)$$

By definition, $F_T \cdot R(t)$ is equal to F_T(ml/min/100g) from time zero to the (vascular) mean transit time, T_c, E is the extraction fraction [108] and k is $F_T E/V_e$ (where V_e is the distribution volume of contrast in the Disse space). The area under the rectangular portion of the blood flow scaled IRF corresponds to the blood volume (V_b, ml/100g). F_a, the hepatic arterial blood flow is then calculated as $\alpha \cdot F_T$ while the permeability surface area product of the liver sinusoids (PS) is calculated via the Renkin and Crone relationship. $PS=-F \cdot \ln(1-E)$.

The calculation of perfusion parameters (T_o, F_T, V_b, F_a and PS) described above is applied to the unique tissue enhancement curve Q(t) corresponding to each voxel in the DCE-CT time series. The model is fit to the measured Q(t) by searching all parameter values and minimizing the sum of squares deviation. All parameter values are constrained to be positive. α and E are fractions and are constrained to be between 0 and 1. Values for the calculated perfusion parameters are then assign to voxels corresponding to the Q(t) from which they were derived. This process generates a two-dimensional functional map for each perfusion parameter corresponding to each slice of the liver in the DCE-CT scan. These maps are displayed as false color images from low (blue) to high (red) functional values.

CT Perfusion is a useful tool in the study of vascular and angiogenic changes that occur in hepatic fibrosis and cirrhosis. It provides a non-invasive means to track

changes in the development of liver disease, and can aid in assessing the effects of treatment as well as prediction of clinical outcomes.

1.7 REASEARCH GOALS

The aim of this project was to evaluate the utility of CT Perfusion in the investigation of fibrotic liver disease. In this regard the three primary goals of this thesis were as follows:

(1) Characterize the bias, variance and covariance of perfusion parameter estimates associated with the CT Perfusion software package.

(2) Track changes in perfusion parameters during the progression of fibrotic liver disease in a rat CCl_4 model of liver fibrosis.

(3) Correlate perfusion parameters in rats measured with CT Perfusion to hepatic fibrosis content at various stages of liver disease.

1.8 THESIS OUTLINE

Chapter 2 presents a study investigating the CT Perfusion software package in terms of the bias, variance and covariance associated with the perfusion parameters estimated. Three different parameter sets corresponding to normal, mild and severe liver disease were used for simulation. My contributions to the study were the determination of parameters sets used, the completion of all mathematical

calculations, setup and running of the Monte Carlo simulations, all subsequent data analysis and interpretation, and the writing and revision of the manuscript.

Chapter 3 presents a study investigating changes in perfusion parameters in a rat CCl_4 model of liver fibrosis in comparison to a control group. Perfusion parameters were also correlated to histology. My contributions to this work were as follows; the handling and treating of the animals with the assistance of a trained animal technician; the conducting of all DCE-CT examinations and subsequent image registration; analysis of the DCE-CT scans with CT Perfusion; performing analysis on the derived functional maps; performing analysis of histological samples; statistical analysis; writing and revising the manuscript.

Chapter 4 provides a summary of the findings from chapter 2 and chapter 3, followed by concluding remarks and suggestions for future work on the evaluation of anti-fibrotic treatments and management of fibrotic liver disease.

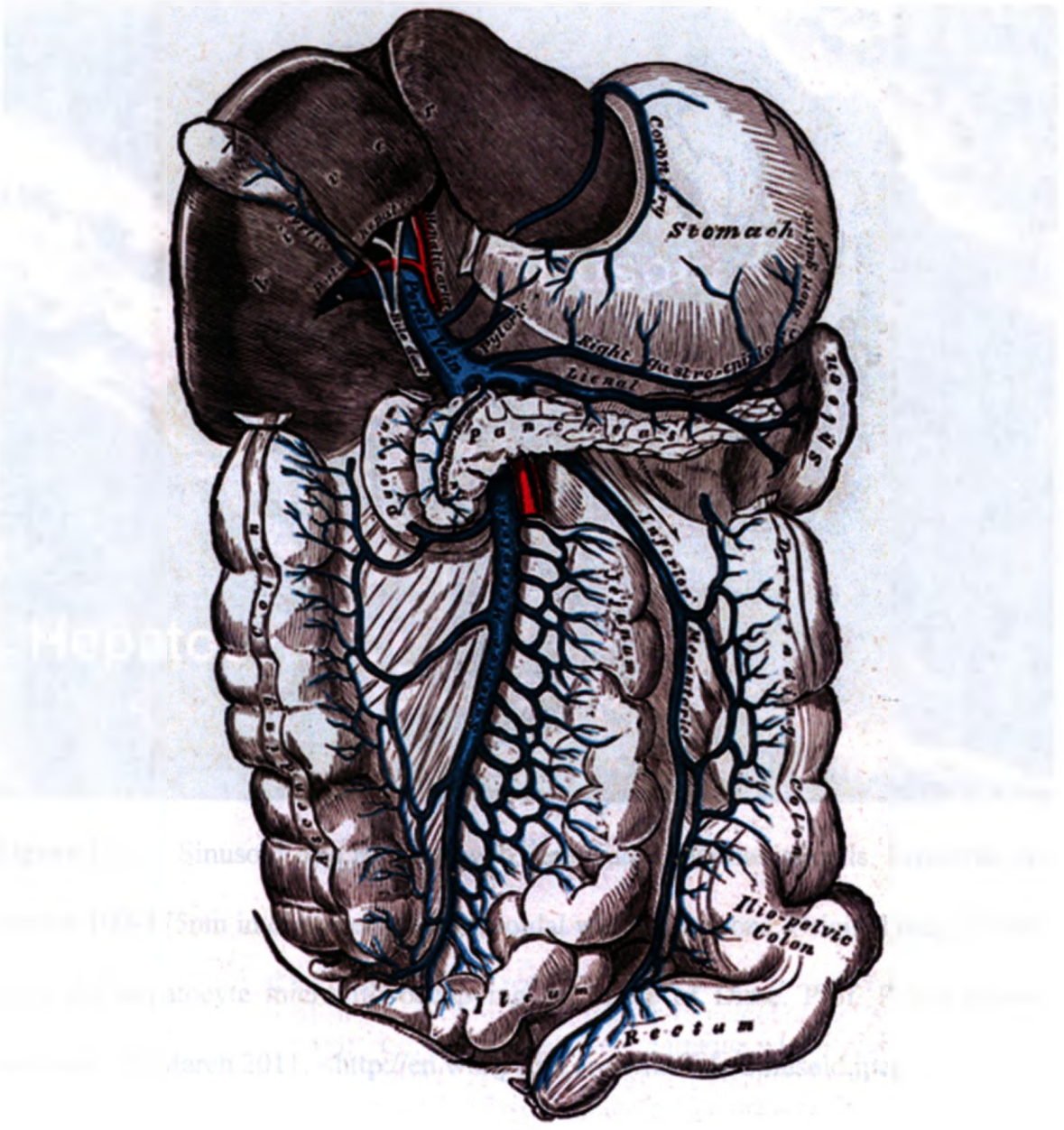

Figure 1.1. Gross anatomy of the gut showing the hepatic artery (red) as well as the portal vein and supplying vessels (blue). The portal vein supplies blood from the spleen, gut and other mesentery, and accounts for approximately 75% of total liver blood flow. The remaining 25% of liver blood flow is supplied from the hepatic artery. Grey's Anatomy. Vein: Hepatic Portal Vein. 28 March 2011. <http://upload.wikimedia.org/wikipedia/commons/3/33/Gray591.png>

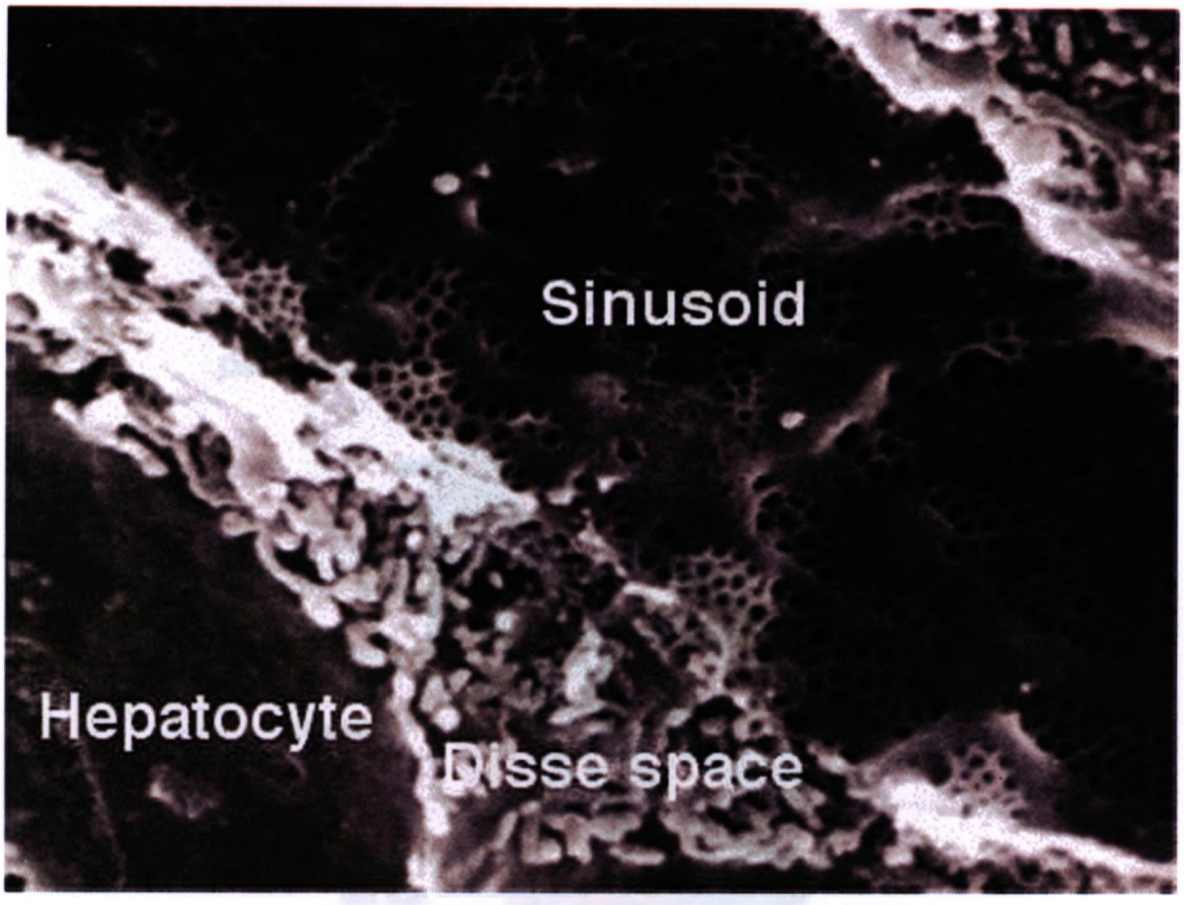

Figure 1.2. Sinusoid of a rat liver with fenestrated endothelial cells. Fenestrae are approx 100-175nm in diameter, and sinusoidal width 5 microns. Original mag 30,000. Note the hepatocyte microvilli occupying the space of Disse. Prof. Robin Fraser. Sinusoid. 28 March 2011. <http://en.wikipedia.org/wiki/File:Sinusoid.jpeg>

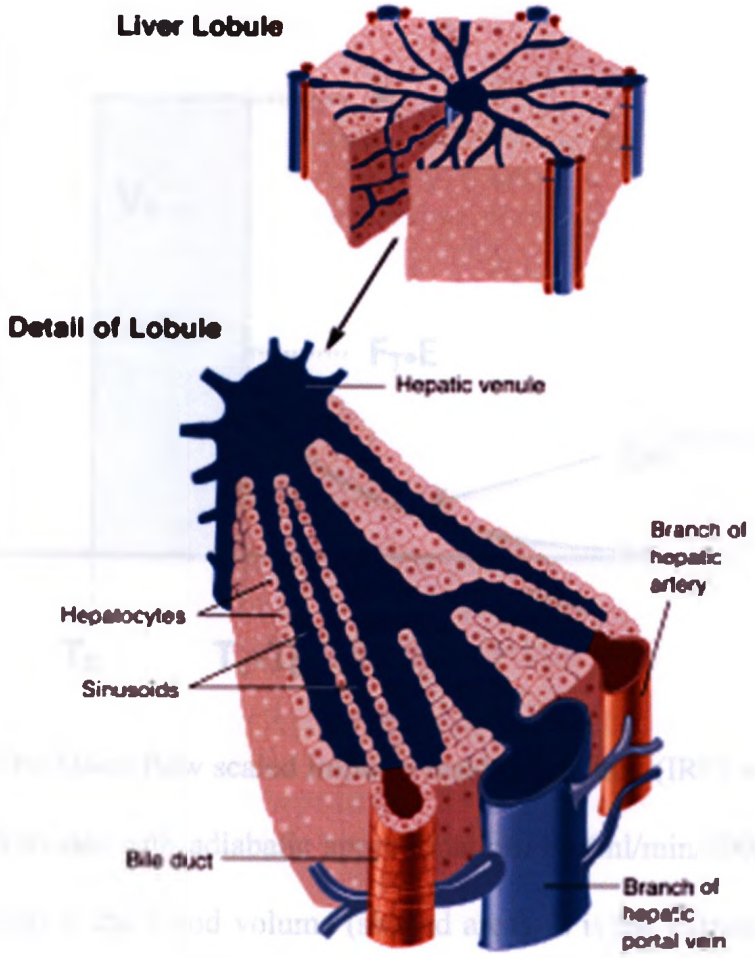

Figure 1.3 The hepatic lobule. Blood flows from the portal triad (hepatic artery, portal vein, bile duct) through the liver sinusoids to a hepatic venule. (Adopted from: Cunningham, C.C., and Van Horn, C.G. Energy availability and alcohol-related liver pathology. Alcohol Research & Health 27(4):281–299, 2003.)

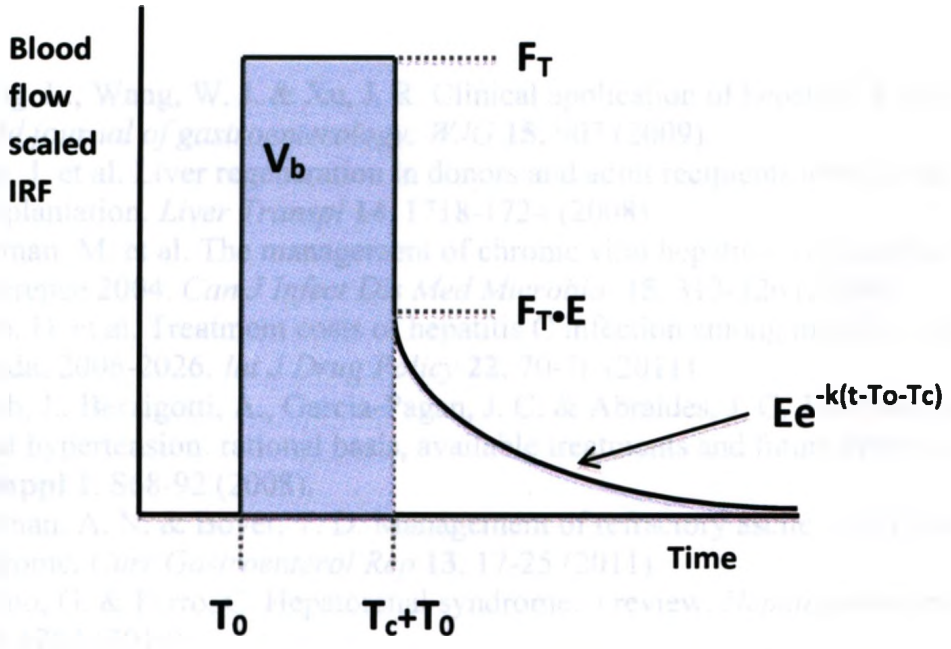

Figure 1.4. The blood flow scaled impulse residue function (IRF) according to the Johnson-Wilson model with adiabatic approximation. F_T (ml/min/100g) is the blood flow, V_b (ml/100g) is the blood volume (shaded area), E is the extraction efficiency, T_c (seconds) is the mean transit time, k is the net back flow rate of the contrast from the extravascular (Disse) space to the intravascular space.

1.9 REFERENCES

1. Zhong, L., Wang, W. J. & Xu, J. R. Clinical application of hepatic CT perfusion. *World journal of gastroenterology: WJG* **15**, 907 (2009).
2. Haga, J. et al. Liver regeneration in donors and adult recipients after living donor liver transplantation. *Liver Transpl* **14**, 1718-1724 (2008).
3. Sherman, M. et al. The management of chronic viral hepatitis: A Canadian consensus conference 2004. *Can J Infect Dis Med Microbiol* **15**, 313-326 (2004).
4. Werb, D. et al. Treatment costs of hepatitis C infection among injection drug users in Canada, 2006-2026. *Int J Drug Policy* **22**, 70-76 (2011).
5. Bosch, J., Berzigotti, A., Garcia-Pagan, J. C. & Abraldes, J. G. The management of portal hypertension: rational basis, available treatments and future options. *J Hepatol* **48 Suppl 1**, S68-92 (2008).
6. Sussman, A. N. & Boyer, T. D. Management of refractory ascites and hepatorenal syndrome. *Curr Gastroenterol Rep* **13**, 17-25 (2011).
7. Testino, G. & Ferro, C. Hepatorenal syndrome: a review. *Hepatogastroenterology* **57**, 1279-1284 (2010).
8. Sass, D. A. & Chopra, K. B. Portal hypertension and variceal hemorrhage. *Med Clin North Am* **93**, 837-53, vii-viii (2009).
9. Tsukuma, H. et al. Risk factors for hepatocellular carcinoma among patients with chronic liver disease. *New England journal of medicine* **328**, 1797-1801 (1993).
10. Braet, F. & Wisse, E. Structural and functional aspects of liver sinusoidal endothelial cell fenestrae: a review. *Comparative Hepatology* **1**, 1 (2002).
11. Wisse, E., De Zanger, R. B., Charels, K., Van Der Smissen, P. & McCuskey, R. S. The liver sieve: considerations concerning the structure and function of endothelial fenestrae, the sinusoidal wall and the space of Disse. *Hepatology* **5**, 683-692 (1985).
12. Gane, E. J. et al. A longitudinal analysis of hepatitis C virus replication following liver transplantation. *Gastroenterology* **110**, 167-177 (1996).
13. Bonnard, P. et al. Documented rapid course of hepatic fibrosis between two biopsies in patients coinfected by HIV and HCV despite high CD4 cell count. *Journal of viral hepatitis* **14**, 806-811 (2007).
14. Gressner, A. M. Transdifferentiation of hepatic stellate cells (Ito cells) to myofibroblasts: a key event in hepatic fibrogenesis. *Kidney international. Supplement* **54**, S39 (1996).
15. Friedman, S. L. Mechanisms of hepatic fibrogenesis. *Gastroenterology* **134**, 1655-1669 (2008).
16. Parola, M. & Robino, G. Oxidative stress-related molecules and liver fibrosis. *Journal of hepatology* **35**, 297-306 (2001).
17. Jaeschke, H. Mechanisms of liver injury. II. Mechanisms of neutrophil-induced liver cell injury during hepatic ischemia-reperfusion and other acute inflammatory conditions. *American Journal of Physiology-Gastrointestinal and Liver Physiology* **290**, G1083 (2006).
18. Jarnagin, W. R., Rockey, D. C., Koteliansky, V. E., Wang, S. S. & Bissell, D. M. Expression of variant fibronectins in wound healing: cellular source and biological

activity of the EIIIA segment in rat hepatic fibrogenesis. *The Journal of cell biology* **127**, 2037 (1994).
19. Canbay, A., Friedman, S. & Gores, G. J. Apoptosis: the nexus of liver injury and fibrosis. *Hepatology* **39**, 273-278 (2004).
20. Canbay, A. et al. Apoptotic body engulfment by a human stellate cell line is profibrogenic. *Laboratory investigation* **83**, 655-663 (2003).
21. Zhan, S. S. et al. Phagocytosis of apoptotic bodies by hepatic stellate cells induces NADPH oxidase and is associated with liver fibrosis in vivo. *Hepatology* **43**, 435-443 (2006).
22. Tsukada, S., Parsons, C. J. & Rippe, R. A. Mechanisms of liver fibrosis. *Clinica chimica acta* **364**, 33-60 (2006).
23. Stefanovic, B., Stefanovic, L., Schnabl, B., Bataller, R. & Brenner, D. A. TRAM2 protein interacts with endoplasmic reticulum Ca2+ pump Serca2b and is necessary for collagen type I synthesis. *Molecular and cellular biology* **24**, 1758 (2004).
24. Pinzani, M. et al. Expression of platelet,Äêderived growth factor in a model of acute liver injury. *Hepatology* **19**, 701-707 (1994).
25. Czochra, P. et al. Liver fibrosis induced by hepatic overexpression of PDGF-B in transgenic mice. *Journal of hepatology* **45**, 419-428 (2006).
26. Melton, A. C. & Yee, H. F. Hepatic stellate cell protrusions couple platelet,Äêderived growth factor,ÄêBB to chemotaxis. *Hepatology* **45**, 1446-1453 (2007).
27. Semela, D. et al. Platelet-derived growth factor signaling through ephrin-b2 regulates hepatic vascular structure and function. *Gastroenterology* **135**, 671-679 (2008).
28. Laleman, W. et al. Both Ca2+-dependent and-independent pathways are involved in rat hepatic stellate cell contraction and intrahepatic hyperresponsiveness to methoxamine. *American Journal of Physiology-Gastrointestinal and Liver Physiology* **292**, G556 (2007).
29. Rockey, D. C. Vascular mediators in the injured liver. *Hepatology* **37**, 4-12 (2003).
30. Melton, A. C., Datta, A. & Yee, H. F. [Ca2+] i-independent contractile force generation by rat hepatic stellate cells in response to endothelin-1. *American Journal of Physiology-Gastrointestinal and Liver Physiology* **290**, G7 (2006).
31. Shah, V. et al. Impaired endothelial nitric oxide synthase activity associated with enhanced caveolin binding in experimental cirrhosis in the rat. *Gastroenterology* **117**, 1222-1228 (1999).
32. Rockey, D. C. Hepatic fibrosis, stellate cells, and portal hypertension. *Clin Liver Dis* **10**, 459-79, vii-viii (2006).
33. Lee, J. S., Semela, D., Iredale, J. & Shah, V. H. Sinusoidal remodeling and angiogenesis: A new function for the liver,Äêspecific pericyte? *Hepatology* **45**, 817-825 (2007).
34. Carmeliet, P. Angiogenesis in life, disease and medicine. *Nature* **438**, 932-936 (2005).
35. Corpechot, C. et al. Hypoxia,Äêinduced VEGF and collagen I expressions are associated with angiogenesis and fibrogenesis in experimental cirrhosis. *Hepatology* **35**, 1010-1021 (2002).
36. Lee, S. et al. Autocrine VEGF signaling is required for vascular homeostasis. *Cell* **130**, 691-703 (2007).
37. Taura, K. et al. Hepatic stellate cells secrete angiopoietin 1 that induces angiogenesis in liver fibrosis. *Gastroenterology* **135**, 1729-1738 (2008).

38. Novo, E. et al. Proangiogenic cytokines as hypoxia-dependent factors stimulating migration of human hepatic stellate cells. *Am J Pathol* **170**, 1942-1953 (2007).
39. Neef, M. et al. Oral imatinib treatment reduces early fibrogenesis but does not prevent progression in the long term. *J Hepatol* **44**, 167-175 (2006).
40. Sato, Y. et al. Resolution of liver cirrhosis using vitamin A,Äìcoupled liposomes to deliver siRNA against a collagen-specific chaperone. *Nature biotechnology* **26**, 431-442 (2008).
41. Issa, R. et al. Spontaneous recovery from micronodular cirrhosis: Evidence for incomplete resolution associated with matrix cross-linking* 1. *Gastroenterology* **126**, 1795-1808 (2004).
42. Desmet, V. J. & Roskams, T. Cirrhosis reversal: a duel between dogma and myth. *Journal of hepatology* **40**, 860-867 (2004).
43. Reiberger, T. et al. Portal Pressure Predicts Outcome and Safety of Antiviral Therapy in Cirrhotic Patients with HCV infection. *Clin Gastroenterol Hepatol* (2011).
44. Choi, G. H. et al. Predictive factors for long-term survival in patients with clinically significant portal hypertension following resection of hepatocellular carcinoma. *Liver Int* **31**, 485-493 (2011).
45. Annet, L. et al. Hepatic flow parameters measured with MR imaging and Doppler US: correlations with degree of cirrhosis and portal hypertension. *Radiology* **229**, 409-414 (2003).
46. Boushel, R. et al. Regional blood flow during exercise in humans measured by near-infrared spectroscopy and indocyanine green. *Journal of Applied Physiology* **89**, 1868 (2000).
47. Burggraaf, J., Schoemaker, H. C. & Cohen, A. F. Assessment of changes in liver blood flow after food intake,Äîcomparison of ICG clearance and echo,ÄêDoppler. *British journal of clinical pharmacology* **42**, 499-502 (1996).
48. Wynne, H. A. et al. The effect of age upon liver volume and apparent liver blood flow in healthy man. *Hepatology* **9**, 297-301 (1989).
49. Norris, C. P., Barnes, G. E., Smith, E. E. & Granger, H. J. Autoregulation of superior mesenteric flow in fasted and fed dogs. *American Journal of Physiology-Heart and Circulatory Physiology* **237**, H174 (1979).
50. Greenway, C. V., Lawson, A. E. & Mellander, S. The effects of stimulation of the hepatic nerves, infusions of noradrenaline and occlusion of the carotid arteries on liver blood flow in the anaesthetized cat. *The Journal of physiology* **192**, 21 (1967).
51. Richardson, P. D. & Withrington, P. G. Pressure-flow relationships and effects of noradrenaline and isoprenaline on the hepatic arterial and portal venous vascular beds of the dog. *J Physiol* **282**, 451-470 (1978).
52. Hughes, R. L., Mathie, R. T., Campbell, D. & Fitch, W. Systemic hypoxia and hyperoxia, and liver blood flow and oxygen consumption in the greyhound. *Pfl√°gers Archiv European Journal of Physiology* **381**, 151-157 (1979).
53. Scholtholt, J. & Shiraishi, T. The reaction of liver and intestinal blood flow to a general hypoxia, hypocapnia and hypercapnia in the anesthetized dog. *Pfl√°gers Arch* **318**, 185-201 (1970).
54. Richardson, P. D. I. & Withrington, P. G. Physiological regulation of the hepatic circulation. *Annual review of physiology* **44**, 57-69 (1982).

55. Lautt, W. W., Legare, D. J. & Ezzat, W. R. Quantitation of the hepatic arterial buffer response to graded changes in portal blood flow. *Gastroenterology* **98**, 1024 (1990).
56. Lautt, W. W. Mechanism and role of intrinsic regulation of hepatic arterial blood flow: hepatic arterial buffer response. *American Journal of Physiology-Gastrointestinal and Liver Physiology* **249**, G549 (1985).
57. Lautt, W. W., Legare, D. J. & d'Almeida, M. S. Adenosine as putative regulator of hepatic arterial flow (the buffer response). *American Journal of Physiology-Heart and Circulatory Physiology* **248**, H331 (1985).
58. Browse, D. J., Mathie, R. T., Benjamin, I. S. & Alexander, B. The role of ATP and adenosine in the control of hepatic blood flow in the rabbit liver in vivo. *Comp Hepatol* **2**, 9 (2003).
59. M√°cke, I., Richter, S., Menger, M. D. & Vollmar, B. Significance of hepatic arterial responsiveness for adequate tissue oxygenation upon portal vein occlusion in cirrhotic livers. *International journal of colorectal disease* **15**, 335-341 (2000).
60. Lloyd, H. G. E. The importance of the transmethylation pathway for adenosine metabolism in the heart. *Topics and Perspectives in Adenosine Research* (1987).
61. Rocheleau, B., Ethier, C., Houle, R., Huet, P. M. & Bilodeau, M. Hepatic artery buffer response following left portal vein ligation: its role in liver tissue homeostasis. *American Journal of Physiology-Gastrointestinal and Liver Physiology* **277**, G1000 (1999).
62. Iwao, T. et al. Hepatic artery hemodynamic responsiveness to altered portal blood flow in normal and cirrhotic livers. *Radiology* **200**, 793-798 (1996).
63. Van Beers, B. E. et al. Hepatic perfusion parameters in chronic liver disease: dynamic CT measurements correlated with disease severity. *American Journal of Roentgenology* **176**, 667 (2001).
64. Aoki, T. et al. Intraoperative direct measurement of hepatic arterial buffer response in patients with or without cirrhosis. *Liver transplantation* **11**, 684-691 (2005).
65. Richter, S., M√°cke, I., Menger, M. D. & Vollmar, B. Impact of intrinsic blood flow regulation in cirrhosis: maintenance of hepatic arterial buffer response. *American Journal of Physiology-Gastrointestinal and Liver Physiology* **279**, G454 (2000).
66. Lautt, W. W. Regulatory processes interacting to maintain hepatic blood flow constancy: Vascular compliance, hepatic arterial buffer response, hepatorenal reflex, liver regeneration, escape from vasoconstriction. *Hepatology Research* **37**, 891-903 (2007).
67. Rappaport, A. M. & Schneiderman, J. H. The function of the hepatic artery. *Ergebnisse der Physiologie, biologischen Chemie und experimentellen Pharmakologie* **76**, 129-175 (1976).
68. Richardson, P. D. I. & Withrington, P. G. The role of Œ≤-adrenoceptors in the responses of the hepatic arterial vascular bed of the dog to phenylephrine, isoprenaline, noradrenaline and adrenaline. *British Journal of Pharmacology* **60**, 239 (1977).
69. Richardson, P. D. & Withrington, P. G. Glucagon inhibition of hepatic arterial responses to hepatic nerve stimulation. *American Journal of Physiology-Heart and Circulatory Physiology* **233**, H647 (1977).

70. Cohen, M. M. & Sitar, D. S. Vasopressin and angiotensin on resistance vessels of spleen, intestine, and liver. *American Journal of Physiology--Legacy Content* **218**, 1704 (1970).
71. Richardson, P. D. & Withrington, P. G. The effects of intra-arterial and intraportal injections of vasopressin on the simultaneously perfused hepatic arterial and portal venous vascular beds of the dog. *Circulation research* **43**, 496 (1978).
72. Onori, P. et al. Hepatic microvascular features in experimental cirrhosis: a structural and morphometrical study in CCl4-treated rats. *Journal of hepatology* **33**, 555-563 (2000).
73. Jenkins, S. A. et al. A dimethylnitrosamine-induced model of cirrhosis and portal hypertension in the rat. *Journal of Hepatology* **1**, 489-499 (1985).
74. Laleman, W. et al. A stable model of cirrhotic portal hypertension in the rat: thioacetamide revisited. *European journal of clinical investigation* **36**, 242-249 (2006).
75. Meijuan, Y. S. B. C. Y. & Liyun, B. J. Z. Comparison between Immunological and Chemical Injury Hepatic Fibrosis Animal Models [J]. *LABORATORY ANIMAL SCIENCE AND ADMINISTRATION* **4**, (1995).
76. Issa, R. et al. Apoptosis of hepatic stellate cells: involvement in resolution of biliary fibrosis and regulation by soluble growth factors. *Gut* **48**, 548 (2001).
77. Tsukamoto, H., Matsuoka, M. & French, S. W. Experimental models of hepatic fibrosis: a review. *Seminars in liver disease* **10(1)**, 56 (1990).
78. Perez, T. R. Is cirrhosis of the liver experimentally produced by CCl4 and adequate model of human cirrhosis? *Hepatology (Baltimore, Md.)* **3**, 112 (1983).
79. Nishikawa, A. et al. Comparative study on organ-specificity of tumorigenicity, mutagenicity and cell proliferative activity induced by dimethylnitrosamine in Big Blue¬Æ mice. *Cancer letters* **117**, 143-147 (1997).
80. Bravo, A. A., Sheth, S. G. & Chopra, S. Liver biopsy. *N Engl J Med* **344**, 495-500 (2001).
81. Bedossa, P., Dargere, D. & Paradis, V. Sampling variability of liver fibrosis in chronic hepatitis C. *Hepatology* **38**, 1449-1457 (2003).
82. Halfon, P. et al. Accuracy of hyaluronic acid level for predicting liver fibrosis stages in patients with hepatitis C virus. *Comp Hepatol* **4**, 6 (2005).
83. Guechot, J. et al. Diagnostic accuracy of hyaluronan and type III procollagen amino-terminal peptide serum assays as markers of liver fibrosis in chronic viral hepatitis C evaluated by ROC curve analysis. *Clin Chem* **42**, 558-563 (1996).
84. Walsh, K. M., Fletcher, A., MacSween, R. N. & Morris, A. J. Basement membrane peptides as markers of liver disease in chronic hepatitis C. *J Hepatol* **32**, 325-330 (2000).
85. Wong, V. S. et al. Serum hyaluronic acid is a useful marker of liver fibrosis in chronic hepatitis C virus infection. *J Viral Hepat* **5**, 187-192 (1998).
86. Park, G. J., Lin, B. P., Ngu, M. C., Jones, D. B. & Katelaris, P. H. Aspartate aminotransferase: alanine aminotransferase ratio in chronic hepatitis C infection: is it a useful predictor of cirrhosis? *J Gastroenterol Hepatol* **15**, 386-390 (2000).
87. Poynard, T. et al. Meta-analyses of FibroTest diagnostic value in chronic liver disease. *BMC Gastroenterol* **7**, 40 (2007).

88. Sandrin, L. et al. Transient elastography: a new noninvasive method for assessment of hepatic fibrosis. *Ultrasound in medicine & biology* **29**, 1705-1713 (2003).
89. Friedrich-Rust, M. et al. Performance of transient elastography for the staging of liver fibrosis: a meta-analysis. *Gastroenterology* **134**, 960-974. e8 (2008).
90. Koizumi, Y. et al. Liver Fibrosis in Patients with Chronic Hepatitis C: Noninvasive Diagnosis by Means of Real-time Tissue Elastography,ÄîEstablishment of the Method for Measurement. *Radiology* **258**, 610 (2011).
91. Grenier, D., Milot, L., Peng, X., Pilleul, F. & Beuf, O. A magnetic resonance elastography (MRE) approach for liver investigation. *Conf Proc IEEE Eng Med Biol Soc* **2007**, 2607-2610 (2007).
92. Kruse, S. A. et al. Tissue characterization using magnetic resonance elastography: preliminary results. *Phys Med Biol* **45**, 1579-1590 (2000).
93. Motosugi, U. et al. Magnetic resonance elastography of the liver: preliminary results and estimation of inter-rater reliability. *Jpn J Radiol* **28**, 623-627 (2010).
94. Yin, M. et al. Assessment of hepatic fibrosis with magnetic resonance elastography. *Clin Gastroenterol Hepatol* **5**, 1207-1213.e2 (2007).
95. Lupsor, M. et al. Analysis of histopathological changes that influence liver stiffness in chronic hepatitis C. Results from a cohort of 324 patients. *J Gastrointestin Liver Dis* **17**, 155-163 (2008).
96. Axel, L. Cerebral blood flow determination by rapid-sequence computed tomography: theoretical analysis. *Radiology* **137**, 679 (1980).
97. Lee, T. Y., Purdie, T. G. & Stewart, E. CT imaging of angiogenesis. *The quarterly journal of nuclear medicine: official publication of the Italian Association of Nuclear Medicine (AIMN)[and] the International Association of Radiopharmacology (IAR)* **47**, 171 (2003).
98. Murphy, B. D. et al. Identification of penumbra and infarct in acute ischemic stroke using computed tomography perfusion-derived blood flow and blood volume measurements. *Stroke* **37**, 1771 (2006).
99. Materne, R. et al. Assessment of hepatic perfusion parameters with dynamic MRI. *Magnetic resonance in medicine* **47**, 135-142 (2002).
100. Miles, K. A. et al. Application of CT in the investigation of angiogenesis in oncology. *Academic radiology* **7**, 840 (2000).
101. Li, X., Benjamin, I. S., Naftalin, R. & Alexander, B. Location and function of intrahepatic shunts in anaesthetised rats. *Gut* **52**, 1339 (2003).
102. Stewart, E. E., Chen, X., Hadway, J. & Lee, T. Y. Hepatic perfusion in a tumor model using DCE-CT: an accuracy and precision study. *Physics in Medicine and Biology* **53**, 4249 (2008).
103. Cenic, A., Nabavi, D. G., Craen, R. A., Gelb, A. W. & Lee, T. Y. A CT method to measure hemodynamics in brain tumors: validation and application of cerebral blood flow maps. *American journal of neuroradiology* **21**, 462 (2000).
104. Purdie, T. G., Henderson, E. & Lee, T. Y. Functional CT imaging of angiogenesis in rabbit VX2 soft-tissue tumour. *Physics in Medicine and Biology* **46**, 3161 (2001).
105. BASSINGTHWAIGHTE, J. B., KNOPP, T. J. & ANDERSON, D. U. Flow estimation by indicator dilution (bolus injection): Reduction of errors due to time-averaged sampling during unsteady flow. *Circulation Research* **27**, 277 (1970).

106. Lawrence, K. S. S. & Lee, T. Y. An adiabatic approximation to the tissue homogeneity model for water exchange in the brain: I. Theoretical derivation. *Journal of Cerebral Blood Flow & Metabolism* **18**, 1365-1377 (1998).
107. Johnson, J. A. & Wilson, T. A. A model for capillary exchange. *The American journal of physiology* **210**, 1299 (1966).
108. Crone, C. & Thompson, A. M. Permeability of brain capillaries. *Capillary Permeability. C. Crone and NA Lassen, editors. Munksgaard, Copenhagen* 447-453 (1970).

CHAPTER 2

ERROR ANALYSIS OF HEPATIC PERFUSION PARAMETERS CALCULATED WITH CT PERFUSION

2.1 INTRODUCTION

In the past, fibrosis and cirrhosis were thought to be irreversible. Newer understanding of the pathogensis of hepatic fibrosis[1,2] has resulted in many potential anti-fibrotic drugs such as the dual endothelin receptor antagonist, Bosentan. In order to test the efficacy of potential anti-fibrotic drugs, a non-invasive measure of fibrosis in animal models and eventually human clinical trials will be required.

The progressive breakdown of normal vascular structure in a cirrhotic liver is associated with an increase in intrahepatic vascular resistance. Consequentially a change in both regional and global perfusion takes place in the liver [3,4]. Patients with cirrhosis have been shown to have a decrease in portal hepatic blood flow (PHBF). The decreased portal perfusion is thought to be partially balanced by an increase in arterial hepatic blood flow (AHBF) via the hepatic arterial buffer response (HABR) [5]. Lautt et. Al. originally demonstrated the HABR in the liver of cats. Richter et. al. demonstrated this process in normal and cirrhotic rat livers and Aoki et. al. later demonstrated it in normal and cirrhotic livers of humans. If PHBF and AHBF can be measured non-invasively, then the change in the ratio of PHBF and AHBF could provide a non-invasive bio-marker for hepatic fibrosis.

Liver perfusion has previously been measured with dynamic PET methods [67].

To properly estimate both PHBF and AHBF a dual input model must be used, requiring arterial and portal time activity curves. Due to the poor spatial resolution of PET images, the portal activity curves cannot be obtained in a non-invasive manor [6].

Doppler ultrasound has also been investigated as a non-invasive method of measuring hepatic blood flow [8]. Doppler ultrasound measures the average velocity of blood (cells) in a vessel, then flow is calculated using an estimate of the cross sectional area of the vessel. This leads to two of the major drawbacks of using Doppler ultrasound. First, blood flow can only be calculated in large vessels, so no regional blood flow information can be obtained. Second, the measure of the cross sectional area depends highly on the skill of the operator, which leads to large intra-observer variability [9].

Both dynamic contrast enhanced computed tomography (DCE-CT) and magnetic resonance imaging (MRI) offer greatly improved resolution over radioisotope techniques, eliminating the need for invasive portal venous measurements. Completely non-invasive measurements of hepatic perfusion can be made and have been shown to correlate well with the severity of cirrhosis [8,10,11]. MRI has the advantage of not exposing patients to potentially harmful ionizing radiation, however, the non-linearity between contrast agent concentration and MRI signal poses problems for quantification.

Using either MRI or CT, several different methods of analysis have been investigated. Miles et al 1993[10] proposed a simple method of measuring blood flow based on the maximum slope of the tissue time density curve (TDC) divided by the peak arterial concentration. Blomley et al 1995[12] reported a modified version that

measures portal venous perfusion by subtracting the splenic time density curve, scaled to represent hepatic arterial flow, from the liver tissue curve. As previously pointed out [13] [14] [15] [16] the maximum slope method has two shortcomings. First, the method assumes no venous outflow of contrast at the time of maximum initial slope, which may not always be true especially in liver disease. Second, modeling techniques allow for the measurement of additional parameters. The maximum slope method only determines arterial and portal venous perfusion, whereas modeling methods can measure additional parameters such as mean vascular transit time (T_c), vascular volume and permeability surface area product (PS). These additional parameters may offer further insight into the development and progression of liver disease.

Matern et al. proposed a dual input compartmental model to estimate both arterial and portal hepatic perfusion. However to achieve the perfusion estimates they assume that the extraction fraction, E, is simply 1.0, meaning that there is no barrier to diffusion between the vascular space and the Space of Disse. This assumption is justified by the fenestrated endothelium of the liver sinusoids, allowing contrast agent to freely diffuse into the extravascular space (EVS). In the normal liver this assumption may be correct, however, capillarization of the sinusoids has been reported in liver fibrosis and cirrhosis [17], which could limit the extraction of contrast agent to the EVS to a varying degree.

The Johnson and Wilson two-compartment model is a good balance between mathematical complexity and accuracy [18]. A time domain solution (the adiabatic approximation) has been proposed and thoroughly investigated for application with oxygen labeled water in the brain as well as treatment planning in stroke with regular

CT contrast [19] [20]. This model has recently been modified for use in the liver by incorporating a dual blood flow source, allowing for the measurement of both PHBF and AHBF, and validated using microspheres in rabbit liver with excellent results [15]. In contrast to the dual input model proposed by Matern et al., the dual input Johnson and Wilson model makes no assumptions on the value of the extraction fraction.

In this study we conduct a sensitivity analysis of the model utilized in CT perfusion (GE Healthcare), as well as Monte Carlo simulations, to investigate the software's utility in the investigation of fibrotic liver disease in a rat model. We consider the normal, mild, and severe stages of liver disease. Hepatic arterial and portal venous input functions used in the analysis and simulations were obtained from actual DCE-CT studies on rats.

2.2 METHODS

2.2.1 Tracer Kinetics Model

Simulations were conducted using CT Perfusion (GE Healthcare). The software utilizes the adiabatic approximation to the Johnson and Wilson model [18] described by St. Lawrence and Lee [19]. A schematic of the model is shown in Figure 2.2, where F_T is the total hepatic blood flow, V_b is the liver blood volume, V_e is the distribution of contrast in the extravascular space of the liver (Space of Disse) and PS is the permeability surface area product of the endothelium of liver sinusoids. The adiabatic approximation solution for the impulse residue function, R(t), of the Johnson and Wilson model can be expressed as follows:

$$R(t)=\begin{cases}0.0 & 0 \le t < T_0 \\ 1.0 & T_0 \le t \le T_0 + T_c \\ Ee^{-k(t-T_0-T_c)} & t > T_0 + T_c\end{cases} \quad (1)$$

where E is the extraction fraction[21] defined as, $E = 1 - e^{-PS/F_T}$, $k=F_TE/V_e$ is the rate constant of the washout of contrast from the EVS to the intravascular space (IVS), T_0 is the time delay between the arrival of contrast at the hepatic artery (or portal vein) and the liver, and T_c is the mean transit time of contrast through the liver vasculature.

For organs with a single blood flow source, such as the brain, the tissue time density curve, Q(t), is defined by Equation 2 [19]. F is the blood flow and C(t) is the time density curve of the supplying vessel.

$$Q(t) = F \cdot C(t) * R(t) \quad (2)$$

For the liver, which derives its blood flow from both the hepatic artery and the portal vein, Q(t) is the sum of the enhancement from both blood flow sources. Thus, Q(t) for the liver becomes:

$$Q(t) = F_a \cdot C_a(t) * R(t) + F_{pv} \cdot C_{pv}(t) * R(t) \quad (3)$$

Where F_a and $C_a(t)$ are the AHBF and the hepatic artery time density curve respectively. Likewise F_{pv} and $C_{pv}(t)$ are PHBF and the portal vein time density curve. R(t) is the same for both F_a and F_{pv} since the same unit of tissue will have the same impulse response function. Equation 3 can be re-written in terms of total blood flow to give Equation 4.

$$Q(t) = F_T \cdot \left[\alpha C_a(t) + (1-\alpha) C_{pv}(t)\right] * R(t) \quad (4)$$

Where F_T is the total hepatic blood flow and α is the fraction of total hepatic blood flow from the hepatic artery.

2.2.2 Sensitivity Analysis

Sensitivity analysis provides a more in-depth understanding of the tracer kinetics model. We calculate the sensitivity functions of each parameter using Equation 5 where, SF_i is the sensitivity function for the i[th] model parameter P_i.

$$SF_i = \frac{\partial Q(t)}{\partial P_i} \tag{5}$$

Each sensitivity function represents the changes in the model output, namely the tissue time density curve (Q(t)), from a small change in the respective parameter. The greater the magnitude of a parameter's sensitivity function, the more sensitive the model output (Q(t)) is to a small change in that parameter and the estimation of that parameter is less affected by noise in Q(t). Also the more similar the sensitivity functions of two parameters are the harder it is to separate the parameters.

2.2.3 Covariance/Correlation Matrix

Calculating the covariance (COV) matrix is important in understanding the inherent variance associated with estimating each of the model parameters. The COV matrix was calculated from the Fisher information matrix, $\bar{F}$, as explained by Huang and Phelps [22] and similarly used by Henderson et. al [23].

Each column of the Fisher information matrix is composed of a different sensitivity function.

$$\tilde{F} = \begin{bmatrix} \frac{\partial Q(t_1)}{\partial F_t} & \frac{\partial Q(t_1)}{\partial \alpha} & \frac{\partial Q(t_1)}{\partial E} & \frac{\partial Q(t_1)}{\partial k} & \frac{\partial Q(t_1)}{\partial T_0} & \frac{\partial Q(t_1)}{\partial T_c} \\ \frac{\partial Q(t_2)}{\partial F_t} & \frac{\partial Q(t_2)}{\partial \alpha} & \frac{\partial Q(t_2)}{\partial E} & \frac{\partial Q(t_2)}{\partial k} & \frac{\partial Q(t_2)}{\partial T_0} & \frac{\partial Q(t_2)}{\partial T_c} \\ \vdots & \vdots & \vdots & \vdots & \vdots & \vdots \\ \frac{\partial Q(t_{n-1})}{\partial F_t} & \frac{\partial Q(t_{n-1})}{\partial \alpha} & \frac{\partial Q(t_{n-1})}{\partial E} & \frac{\partial Q(t_{n-1})}{\partial k} & \frac{\partial Q(t_{n-1})}{\partial \partial T_0} & \frac{\partial Q(t_{n-1})}{\partial T_c} \\ \frac{\partial Q(t_n)}{\partial F_t} & \frac{\partial Q(t_n)}{\partial \alpha} & \frac{\partial Q(t_n)}{\partial E} & \frac{\partial Q(t_n)}{\partial k} & \frac{\partial Q(t_n)}{\partial T_0} & \frac{\partial Q(t_n)}{\partial T_c} \end{bmatrix} \quad (6)$$

The covariance matrix is:

$$COV = \sigma^2 \cdot \left[\tilde{F}^T \cdot \tilde{F}\right]^{-1} \quad (7)$$

where σ^2 is the estimate of the noise variance in the measured model output, Q(t).

The diagonal elements of the covariance matrix are the variances (σ_i^2 i=F_t, α, E, k, T_0 and T_c) of the estimated parameters from the model. The off diagonal elements are the covariances (σ_{ij}^2 i,j=F_T, α, E, k, T_0 and T_c) of two estimated parameters. The covariance matrix can be converted into the correlation matrix.

$$P_{ij} = \frac{\sigma_{ij}^2}{\sigma_i \sigma_j} \quad (8)$$

Elements of the correlation matrix are all between -1 and 1. Unity represents perfect positive correlation and -1 is perfect negative correlation. A coefficient of zero represents no correlation. The correlation matrix allows for an easier interpretation of parameter interactions.

2.2.4 Monte Carlo Simulation

Three different states of disease severity were considered for simulation. Table 1 lists the parameter values for normal, mild and severe liver fibrosis. The values for α,

F, E, k, T_o, and T_c were estimated from microsphere experiments and indicator dilution techniques in rats [24 25 26]. Total hepatic blood volume, V_b and PS were derived from the assumed parameter values as $V_b=F\cdot T_c$ according to the Central Volume Principle [27,28] and $PS=-F_T\cdot\ln(1-E)$ from the Crone relationship [21]. Using the assumed parameter values of each disease state, along with the arterial and portal venous time density curves in Figure 2.1, the tissue TDC, Q(t), can be calculated using Equation 1 and Equation 4. Gaussian random noise, which standard deviation was equal to the square root of Q(t), was added to the tissue TDC.

For each disease state a time series of simulated CT images were generated from the simulated noisy curves of the corresponding tissue TDC. Each set of images consisted of a 48x48 pixel block where the time density curve of a pixel was a simulated noisy curve of the corresponding tissue TDC. CT Perfusion was used to analyze each set of images to estimate the different parameters and their differences from the 'true' values. This method resulted in the equivalent of 2304 simulation runs per simulated tissue TDC. From this data the variance and bias of each estimated parameter was determined.

3.3 RESULTS

Figure 2.3 shows the sensitivity functions calculated from Equation 1 for each parameter of the model as well as for each disease condition, normal, mild, and severe. Total blood flow was the most sensitive parameter followed by α, k, E, T_c, and T_0 respectively. The sensitivity of total blood flow increased with increasing

disease severity while the sensitivity of α decreased. E and k both exhibited low sensitivity in the first 30 seconds, followed by increased sensitivity in the later phase. The mean transit time, T_c, showed decreasing sensitivity with increasing disease severity. The sensitivity of T_0 showed little change with disease severity.

Table 2 lists the variances of the estimated model parameters under normal, mild, and severe disease conditions, as determined from the diagonal of the covariance matrix. The variances of V_b and PS were calculated from those of other parameters using standard error propagation techniques. As disease severity increased all estimated parameters showed a decrease in their variation except α, which showed a slight increasing trend.

The correlation matrix was calculated for each disease severity and is shown in Table 3. (α) was highly correlated with T_0 for normal and mild disease states as well as F_T for mild and sever disease states. The highest correlations were observed between F_T and T_c as well as between E and k.

Figure 2.4 show the results from the Monte Carlo simulations. The bias is plotted on the vertical axis and standard deviation of the added Gaussian noise on the horizontal axis. Error bars represent the standard deviation of the estimated biases at each level of noise. T_0 and V_b showed little change in bias for both increasing noise and disease severity. Bias remained stable for T_c and F_T estimates for the mild and severe disease states but increased with noise for the normal disease state. The accuracy of parameter estimation amongst all parameters tended to decrease with increasing noise. The accuracy of estimating T_0 and T_c increased with increasing disease severity while α estimates showed decreasing accuracy with increased disease

severity.

3.4 DISCUSSION

To evaluate the utility of CT-Perfusion software in assessing changes in a rat model fibrotic liver disease, we conducted a sensitivity analysis of the Johson and Wilson model utilized by CT-Perfusion as well as performed Monte-Carlo simulations for normal, mild and severe disease conditions as outlined in Table 1.

In the Monte-Carlo simulations T_0 estimates were very stable, showing little bias among all disease states and noise levels. As predicted by the covariance matrix the variance of the estimate decreased with increasing disease level.

Monte-Carlo simulations for T_c showed a positive bias under the normal condition. Mild and sever disease conditions showed little bias. The correlation matrix showed a strong negative correlation between T_c and F_T. In the Monte-Carlo simulations the estimates of F_T was negatively biased for normal conditions. Thus, the Monte Carlo simulations demonstrate the strong negative correlation between T_c and F_T predicted by the covariance/correlation matrix. The variances of T_c and F_T in the Monte Carlo simulations also agreed with the predictions of the covariance matrix, both decreased with increasing disease severity.

The V_b estimates in the Monte Carlo simulations were stable among disease states and noise levels. The mild diseased state had the largest bias but still remained less than 10% relative to the mean. The V_b estimates also had the smallest variance of all the estimated parameters relative to their means. This is likely because of the

strong negative correlation between T_c and F_T. Since V_b is the product of T_c and F_b according to the Central Volume Principle[27,28], any error in one parameter would largely be canceled out by error in the other.

Determined by F_T and E via Crone's equation [21], PS was the least stable and accurate of all the parameters. This should not be surprising as the covariance matrix predicted a very large variance for the estimation of PS. As the Monte-Carlo simulations demonstrate in Figure 2.4, constraints applied by CT Perfusion software greatly reduce this variance. Consequentially a large bias is introduced into the estimate. The changes in the sensitivity function of E over disease severities were the largest among all the parameters (Figure 2.3 C). These changes in sensitivity also affect the parameters with which E is correlated. Under normal conditions E is partially correlated with T_c, but then becomes more closely correlated with α and F_T as the disease severity worsens. These correlations mean that any bias in E will be transferred to the correlated parameters. Thus, bias in the estimate of E, which is caused by constraints intended to reduce its variance in CT Perfusion, is a major source of bias seen in the other parameters.

The covariance matrix showed no trend in the variance of α, however, in the Monte-Carlo simulations the variance for α increased as disease severity worsens. This is likely due to the physiological constraint that α must be positive which is employed by CT-Perfusion. At low values of α this constraint will affect the estimate more than at the higher values. As a result the low α (low disease severity) estimates have lower variance than predicted by the covariance matrix. Overall the Monte-Carlo simulations show a stable estimate of α with disease severity and noise levels.

Variance, although increasing with disease severity, remained reasonable. The sensitivity function for α shows a narrow temporal window of sensitivity. Care should be taken that no motion or other artifacts occur during this window of imaging or large errors in the estimation of α may result.

We conducted a sensitivity analysis of the model utilized by CT-Perfusion, as well as performed Monte-Carlo simulations for different health conditions, both normal and abnormal, of the liver. The comparison of the theoretical estimates of variance from the covariance matrix to the results of the Monte-Carlo simulations highlight some of the effects of constraints used in CT-Perfusion software. While constraining a variable can reduce its variance, this inevitably introduces a bias into the estimate. Whenever there is a high level of correlation between parameters, caution should be used when applying constraints. Any bias introduced by a constraint will not only bias the constrained parameter, but can bias other correlated parameters as well.

There are limitations in this study. First, one set of the arterial and the portal venous time density curves from a single DCE-CT rat study was used to generate the Monte-Carlo simulations as well as the sensitivity functions and covariance and correlation matrices. Second, the effects of different noise levels of the input time density curves or injection rates were not investigated. The effect of different injection rates on compartmental models has been investigated several times before [14] [23] [29]. It has been concluded that slowing down the injection rate generally increases uncertainty and bias in parameter estimation.

Overall these simulations suggest that CT-Perfusion can accurately and reliably measure multiple physiological parameters in the liver of the rat. One of these parameters, α, being the ratio between the F_a and F_T, could be a sensitive parameter for non-invasively measuring fibrosis progression in the liver.

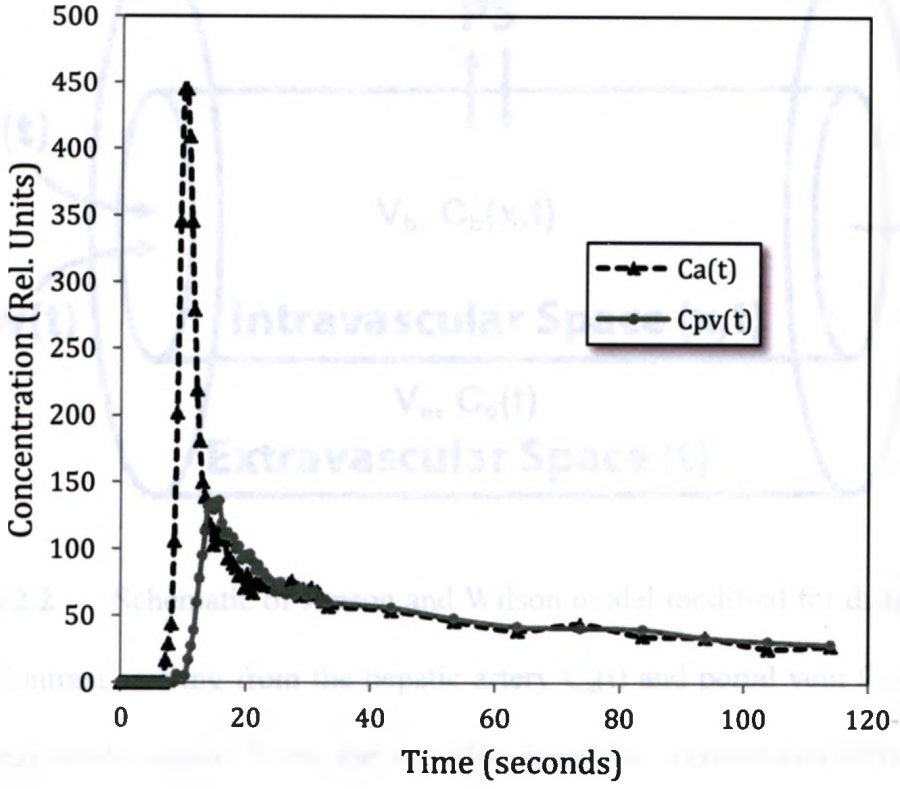

Figure 2.1 Time density (concentration) curves of the abdominal aorta, Ca(t), and the portal vein, Cpv(t), acquired from a DCE- CT study on a rat scanned at 120kVp and 80mA.

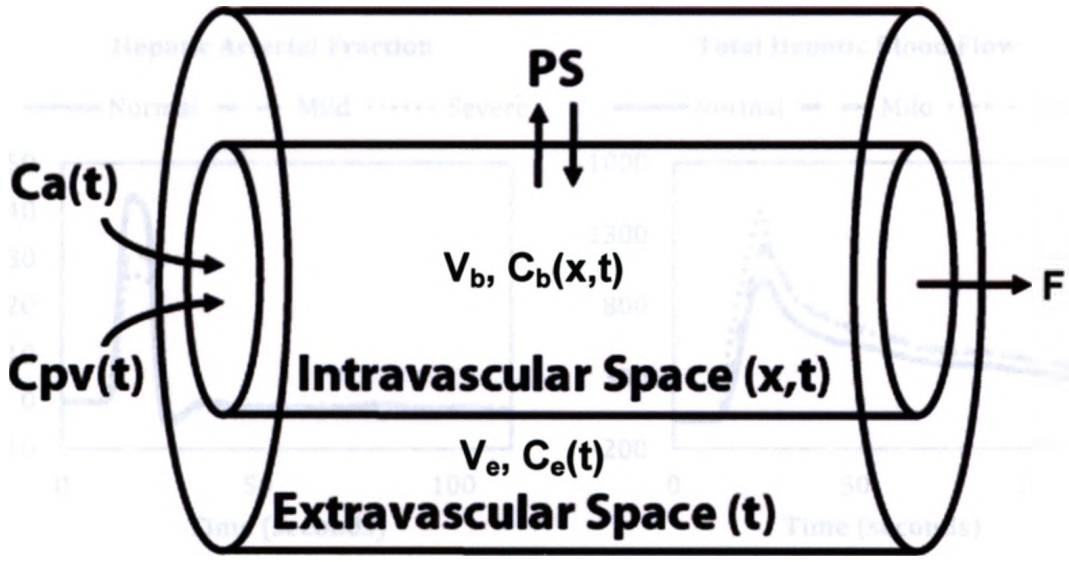

Figure 2.2 Schematic of Jonson and Wilson model modified for dual input for the liver. Contrast arriving from the hepatic artery $C_a(t)$ and portal vein $C_{pv}(t)$ flows into the intravascular space. From the vascular space the contrast can diffusion into the extravascular (Disse) space.

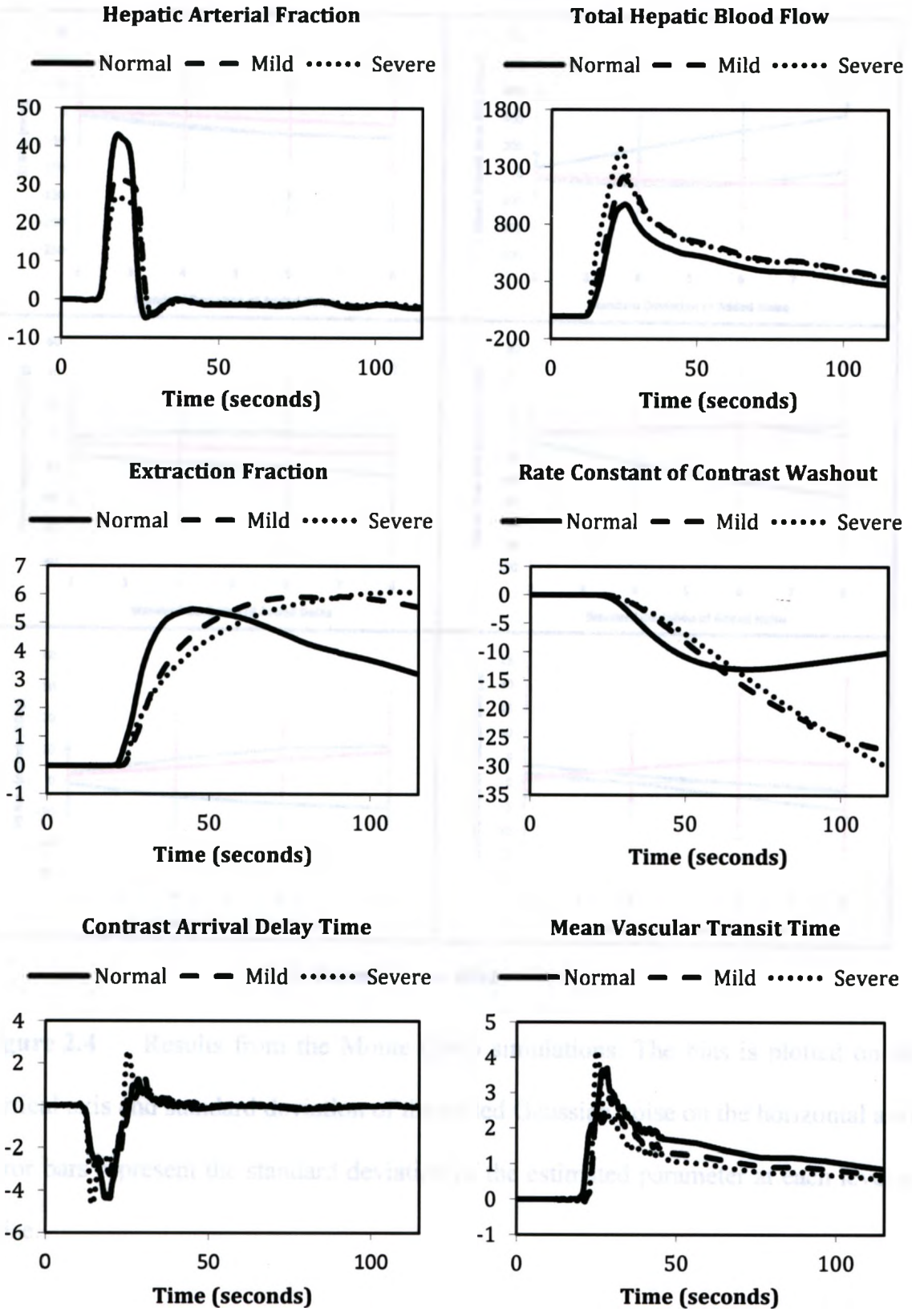

Figure 2.3 Sensitivity functions for normal, mild, and severe disease conditions.

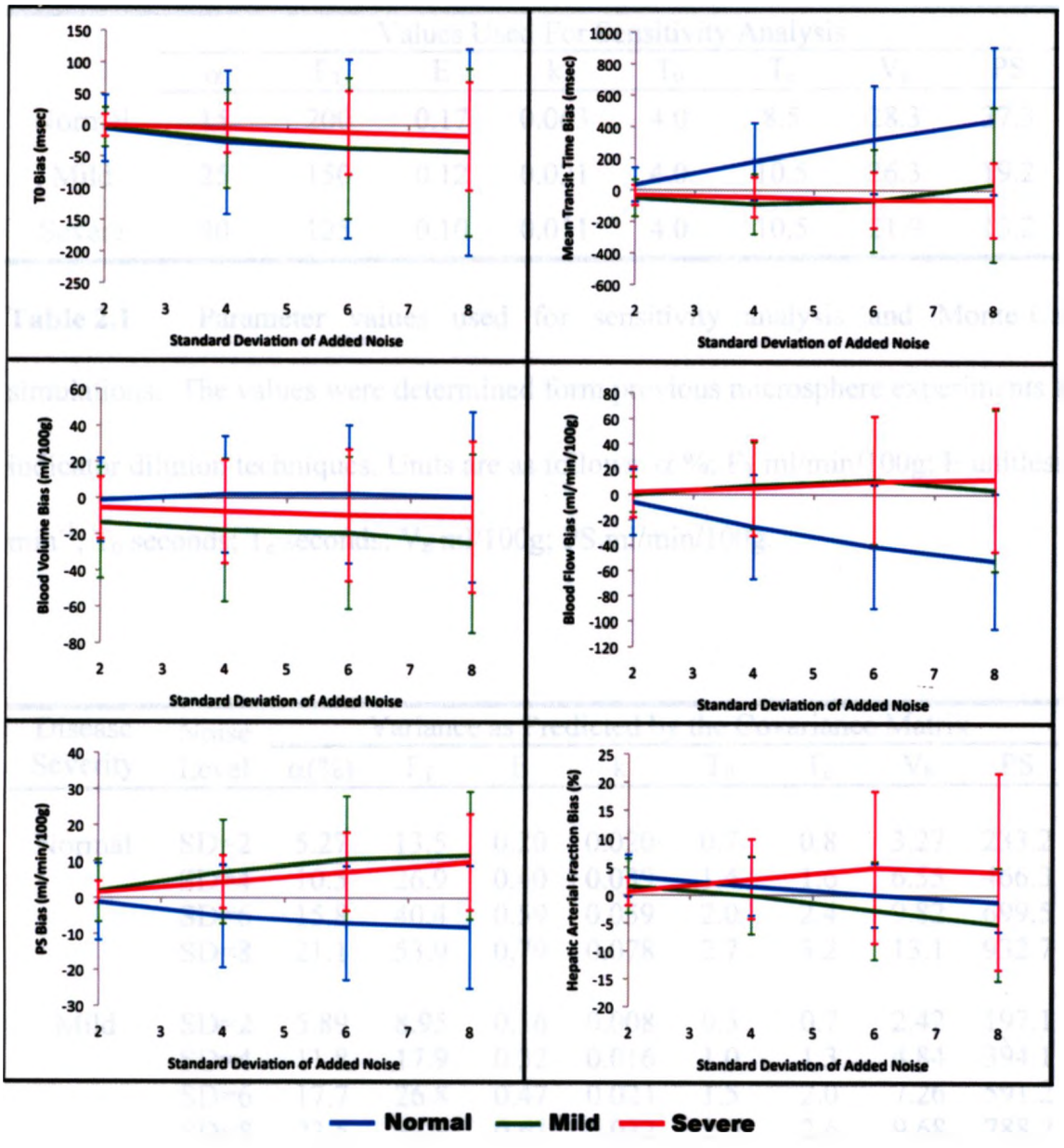

Figure 2.4 Results from the Monte Carlo simulations. The bias is plotted on the vertical axis and standard deviation of the added Gaussian noise on the horizontal axis. Error bars represent the standard deviation of the estimated parameter at each level of noise.

	Values Used For Sensitivity Analysis							
	α	F_T	E	k	T_0	T_c	V_b	PS
Normal	15	200	0.17	0.063	4.0	8.5	28.3	37.3
Mild	25	150	0.12	0.021	4.0	10.5	26.3	19.2
Severe	40	125	0.10	0.011	4.0	10.5	21.9	13.2

Table 2.1 Parameter values used for sensitivity analysis and Monte-Carlo simulations. The values were determined form previous microsphere experiments and indicator dilution techniques. Units are as follows: α %; F_T ml/min/100g; E unitless; k min^{-1}; T_0 seconds; T_c seconds; V_b ml/100g; PS ml/min/100g.

Disease Severity	Noise Level	Variance as Predicted by the Covariance Matrix							
		α(%)	F_T	E	k	T_0	T_c	V_b	PS
Normal	SD=2	5.27	13.5	0.20	0.020	0.7	0.8	3.27	233.2
	SD=4	10.5	26.9	0.40	0.039	1.4	1.6	6.55	466.3
	SD=6	15.8	40.4	0.59	0.059	2.0	2.4	9.82	699.5
	SD=8	21.1	53.9	0.79	0.078	2.7	3.2	13.1	932.7
Mild	SD=2	5.89	8.95	0.16	0.008	0.5	0.7	2.42	197.1
	SD=4	11.8	17.9	0.32	0.016	1.0	1.3	4.84	394.1
	SD=6	17.7	26.8	0.47	0.024	1.5	2.0	7.26	591.2
	SD=8	23.5	35.8	0.63	0.032	2.0	2.6	9.68	788.2
Severe	SD=2	5.32	7.54	0.17	0.006	0.3	0.6	1.88	216.3
	SD=4	10.6	15.1	0.35	0.012	0.7	1.1	3.76	432.6
	SD=6	16.0	22.6	0.52	0.018	1.0	1.7	5.65	648.9
	SD=8	21.3	30.2	0.69	0.024	1.3	2.3	7.53	865.2

Table 2.2 Variances of estimated parameters for normal, mild, and severe liver disease, as determined from the diagonal of the covariance matrix. Units are as follows: α %; F_T ml/min/100g; E unitless; k min^{-1}; T_0 seconds; T_c seconds; V_b ml/100g; PS ml/min/100g.

Disease Severity		Correlation Matrix					
		α	F_T	E	k	T_0	T_c
Normal	α	1.000	0.027	0.137	-0.186	0.870	-0.147
	F_T	0.027	1.000	0.264	0.222	0.476	-0.948
	E	0.137	0.264	1.000	0.883	0.224	-0.500
	K	-0.186	0.222	0.883	1.000	-0.078	-0.360
	T_0	0.870	0.476	0.224	-0.078	1.000	-0.554
	T_c	-0.147	-0.948	-0.500	-0.360	-0.554	1.000
		α	F_T	E	k	T_0	T_c
Mild	α	1.000	-0.623	0.576	0.310	0.793	0.322
	F_T	-0.623	1.000	-0.305	-0.116	-0.079	-0.895
	E	0.576	-0.305	1.000	0.908	0.511	-0.086
	K	0.310	-0.116	0.908	1.000	0.306	-0.173
	T_0	0.793	-0.079	0.511	0.306	1.000	-0.232
	T_c	0.322	-0.895	-0.086	-0.173	-0.232	1.000
		α	F_T	E	k	T_0	T_c
Severe	α	1.000	-0.748	0.690	0.511	0.570	0.420
	F_T	-0.748	1.000	-0.534	-0.380	0.018	-0.861
	E	0.690	-0.534	1.000	0.939	0.425	0.110
	K	0.511	-0.380	0.939	1.000	0.330	0.027
	T_0	0.570	0.018	0.425	0.330	1.000	-0.364
	T_c	0.420	-0.861	0.110	0.027	-0.364	1.000

Table 2.3 Correlation matrices of estimated parameters for normal, mild, and severe liver disease. Elements of the correlation matrix are all between -1 and 1. Unity represents perfect positive correlation and -1 is perfect negative correlation. A coefficient of zero represents no correlation.

2.5 REFRENCES

1. Bonis, P. A. L., Friedman, S. L. & Kaplan, M. M. Is liver fibrosis reversible? *New England Journal of Medicine* **344**, 452-454 (2001).
2. Desmet, V. J. & Roskams, T. Cirrhosis reversal: a duel between dogma and myth. *Journal of hepatology* **40**, 860-867 (2004).
3. Van Beers, B. E. et al. Hepatic perfusion parameters in chronic liver disease: dynamic CT measurements correlated with disease severity. *American Journal of Roentgenology* **176**, 667 (2001).
4. Tsushima, Y., Blomley, M. J. K., Kusano, S. & Endo, K. The portal component of hepatic perfusion measured by dynamic CT (an indicator of hepatic parenchymal damage). *Digestive diseases and sciences* **44**, 1632-1638 (1999).
5. Richter, S., M√°cke, I., Menger, M. D. & Vollmar, B. Impact of intrinsic blood flow regulation in cirrhosis: maintenance of hepatic arterial buffer response. *American Journal of Physiology-Gastrointestinal and Liver Physiology* **279**, G454 (2000).
6. Ziegler, S. I. et al. Measurement of liver blood flow using oxygen-15 labelled water and dynamic positron emission tomography: limitations of model description. *European Journal of Nuclear Medicine and Molecular Imaging* **23**, 169-177 (1996).
7. Iwasa, M. et al. Single photon emission computed tomography to determine effective hepatic blood flow and intrahepatic shunting. *Hepatology* **21**, 359-365 (1995).
8. Annet, L. et al. Hepatic flow parameters measured with MR imaging and Doppler US: Correlations with degree of cirrhosis and portal hypertension1. *Radiology* **229**, 409 (2003).
9. Colli, A. et al. Severe Liver Fibrosis or Cirrhosis: Accuracy of US for Detection,ÄîAnalysis of 300 Cases1. *Radiology* **227**, 89 (2003).
10. Miles, K. A., Hayball, M. P. & Dixon, A. K. Functional images of hepatic perfusion obtained with dynamic CT. *Radiology* **188**, 405 (1993).
11. Materne, R. et al. Assessment of hepatic perfusion parameters with dynamic MRI. *Magnetic resonance in medicine* **47**, 135-142 (2002).
12. Blomley, M. J. K. et al. Liver perfusion studied with ultrafast CT. *Journal of computer assisted tomography* **19**, 424 (1995).
13. VAN BEERS, B. Non-invasive quantification of liver perfusion with dynamic computed tomography and a dual-input one-compartmental model. *Clinical Science* **99**, 517-525 (2000).
14. Miyazaki, S., Yamazaki, Y. & Murase, K. Error analysis of the quantification of hepatic perfusion using a dual-input single-compartment model. *Physics in Medicine and Biology* **53**, 5927 (2008).
15. Stewart, E. E., Chen, X., Hadway, J. & Lee, T. Y. Hepatic perfusion in a tumor model using DCE-CT: an accuracy and precision study. *Physics in Medicine and Biology* **53**, 4249 (2008).

16. Lee, T. Y., Purdie, T. G. & Stewart, E. CT imaging of angiogenesis. *The quarterly journal of nuclear medicine: official publication of the Italian Association of Nuclear Medicine (AIMN)[and] the International Association of Radiopharmacology (IAR)* **47**, 171 (2003).
17. Fukuda, Y., Nagura, H., Imoto, M. & Koyama, Y. Immunohistochemical studies on structural changes of the hepatic lobules in chronic liver diseases. *The American journal of gastroenterology* **81**, 1149 (1986).
18. Johnson, J. A. & Wilson, T. A. A model for capillary exchange. *The American journal of physiology* **210**, 1299 (1966).
19. Lawrence, K. S. S. & Lee, T. Y. An adiabatic approximation to the tissue homogeneity model for water exchange in the brain: II. Experimental validation. *Journal of Cerebral Blood Flow & Metabolism* **18**, 1378-1385 (1998).
20. Murphy, B. D. et al. White Matter Thresholds for Ischemic Penumbra and Infarct Core in Patients with Acute Stroke: CT Perfusion Study1. *Radiology* **247**, 818 (2008).
21. Crone, C. The permeability of capillaries in various organs as determined by use of the ‚Äòindicator diffusion‚Äômethod. *Acta Physiologica Scandinavica* **58**, 292-305 (1963).
22. Huang, S. C. & Phelps, M. E. Error in parameter estimates with variations in flow: measurement of oxygen utilization with positron-emission tomography. *Circulation* **72**, IV77 (1985).
23. Henderson, E., Rutt, B. K. & Lee, T. Y. Temporal sampling requirements for the tracer kinetics modeling of breast disease. *Magnetic resonance imaging* **16**, 1057-1073 (1998).
24. Goresky, C. A. A linear method for determining liver sinusoidal and extravascular volumes. *American Journal of Physiology--Legacy Content* **204**, 626 (1963).
25. Groszmann, R. J., Vorobioff, J. & Riley, E. Splanchnic hemodynamics in portal-hypertensive rats: measurement with gamma-labeled microspheres. *American Journal of Physiology-Gastrointestinal and Liver Physiology* **242**, G156 (1982).
26. Conzen, P. F. et al. Systemic and regional hemodynamics of isoflurane and sevoflurane in rats. *Anesthesia & Analgesia* **74**, 79 (1992).
27. Celsis, P. et al. Measurement of cerebral circulation time in man. *European Journal of Nuclear Medicine and Molecular Imaging* **10**, 426-431 (1985).
28. Meier, P. & Zierler, K. L. On the theory of the indicator-dilution method for measurement of blood flow and volume. *Journal of applied physiology* **6**, 731 (1954).
29. Murase, K. & Miyazaki, S. Error analysis of tumor blood flow measurement using dynamic contrast-enhanced data and model-independent deconvolution analysis. *Physics in Medicine and Biology* **52**, 2791 (2007).

CHAPTER 3

IN-VIVO MONITORING OF THE DEVELOPMENT AND PROGRESSION OF HEPATIC FIBROSIS IN A CCl_4 RAT MODEL WITH CT PERFUSION

3.1 INTRODUCTION

With an increased understanding of the mechanism of fibrosis in response to chronic liver injury[1], potential anti-fibrotic drugs have been proposed and demonstrated the reversal of liver fibrosis in-vitro and in-vivo[2 3 4]. To effectively test these drugs, both in animals and eventually in clinical trials, a repeatable measure of fibrosis progression will be required.

The staging of fibrosis is also an important factor in treatment planning. Patients with hepatitis C virus have been shown to benefit from antiviral therapy however; interferon treatment is not without its complications [5 6 7]. Thus, therapy is reserved for those who have already shown a marked progression of liver disease. Currently patients with a METAVIR score [8] of F2 or F3 are classified as having 'clinically significant' fibrosis meaning they are at higher risk for developing cirrhosis and it's subsequent complications. Thus, patients with clinically significant fibrosis have a higher indication for anti-viral treatment than patients with no, or minimal fibrosis (METAVIR F0/F1) [9 10]. Patients with the highest METAVIR score of F4 should be monitored and treated for cirrhosis related complications such as, portal hypertension and hepatocellular carcinoma.

Liver biopsy is currently the gold standard for assessing fibrosis, however it is not without limitations. Histological grading is not reproducible; there are both intra- and inter-observer variability on small sized or fragmented biopsy samples[11]. In addition the biopsy procedure can be painful and carries a risk of serious complications[12], greatly reducing patients' willingness to participate in clinical trials. Because of these limitations, biopsy is an impractical method for the regular monitoring of liver fibrosis required for the evaluation of new anti-fibrotic treatments as well as treatment planning.

In response to this need, many noninvasive methods for monitoring hepatic fibrosis have been proposed; of which the most thoroughly investigated is serum markers. Both direct serum markers, such as hyaluronate, and indirect serum markers such as alanine transaminase (ALT) and aspartate transaminase (AST) have been investigated [13] [14] [15] [16] [17]. When only direct or indirect markers are used individually they can reasonably diagnosis or exclude cirrhosis but lack the ability to differentiate intermediate stages of fibrosis. Thus newer algorithms, combining multiple markers, such as Fibrotest or the Enhanced Liver Fibrosis (ELF) test have been proposed to improve diagnostic accuracy. In a meta-analysis Fibrotest was able to distinguish between METAVIR stages ≤F1 vs ≥F2 or 'clinically significant' fibrosis with AUROC of .84 [18]. A limitation of direct liver markers is that they are not liver specific thus; they require patient specific considerations to be taken into account when interpreting the results. Currently, the ability to measure direct markers is not routinely available in most hospitals.

Non-invasive imaging methods for staging of liver fibrosis have been proposed as well. Some of these include, diffusion-weighted magnetic resonance (MR)[19 20 21], liver stiffness measurement (LSM) techniques such as transient elastography[22,23] and MR elastography[24 25 26], as well as perfusion imaging [27-29].

The goal of perfusion imaging in the liver is to track changes in the hepatic microvasculature. Chronic liver disease, regardless of the etiology, leads to the "activation" of hepatic stellate cells[30]. This activation results in the transition of the quiescent hepatic stellate cells to a proliferative, fibrogenic, and contractile myofibroblast-like phenotype. The contractility of the activated hepatic stellate cells, as well as the resulting fibro-genesis and collagen deposition, disrupts the normal sinusoidal vasculature. Consequentially, an increase in blood flow resistance is observed leading to decreased portal blood perfusion and portal hypertension[31].

In this regard the aim of our study was to correlate the perfusion parameters calculated using CT-Perfusion (GE Healthcare) in the liver of the rat, to the amount of liver fibrosis determined by digital image analysis of stained excised liver sections.

3.2 METHODS

3.2.1 Animal Model

Male Sprague-Dawley rats (300g - 350g) were randomized into control and treated groups. To induce liver cirrhosis, the treated group (n=9) received intraperitoneal injections of carbon tetra-chloride (CCl_4) three times a week at a dose of 0.15ml/kg diluted 1:6 in olive oil. Phenobarbital (0.04g/L) was also added to the

drinking water of the CCl_4 treated animals to further potentiate liver damage [32]. The control group (n=6) received intraperitoneal saline injections three times a week. Dynamic contrast enhance computed tomography (DCE-CT) scans, as described below, were performed on all animals at baseline and after 2, 4, 6, and 8 weeks of treatment. After 8 weeks of treatment all animals were euthanized. Livers were removed and fixed in 10% buffered formalin for histological examination.

To obtain histology samples at intermediate disease levels two groups of rats were treated with CCl_4 and phenobarbital as described above. The first group (n=5) received treatment for 4 weeks and the second group (n=5) received treatment for 6 weeks. After the respective 4 and 6 weeks of treatment, DCE-CT scans were performed. The animals were then euthanized and livers were removed for histological analysis.

3.2.2 Animal Preparation

Animals were initially sedated with 3% isoflurane. Once sedated, a catheter was inserted into the tail vein. 35mg/kg of pentobarbital was then administered via intra-venous (IV) injection and isoflurane anesthesia was discontinued. Animals were then intubated and placed in a supine position of the CT bed where they were mechanically ventilated on oxygen at a rate of approximately 80 breaths per minute. To facilitate a breath hold, 0.1ml/kg of the paralytic, pancuronium, was administered IV just prior to imaging. CO_2 and O_2 levels were monitored using a pulse oximeter. PCO_2 was maintained at 40+/-2 mm Hg and O_2 saturation was maintained above 98%. Temperature was monitored via rectal probe and maintained at 37.5 +/- 0.5C with a

re-circulating heated water blanket. Supplemental doses (5mg/kg) of pentobarbital were administered IV as required during the experiment.

3.2.3 Imaging

DCE-CT scans were performed using a clinical GE multi-slice CT scanner (Discovery VCT, GE Healthcare). A localization scan was first performed to place eight 5mm slices covering the entire liver. After the scan location was selected the DCE-CT scan was conducted in two phases. In the first phase, images were acquired in cine mode with a tube voltage and current of 120kVp and 80mA respectively and a gantry speed of one rotation per second. Images were reconstructed using the detail filter and a temporal resolution of 0.45 seconds. Total time for the first phase cine scan was 34 seconds. At the beginning of the scan 1ml/kg of an iodinated contrast agent (Omnipaque 300mgI/ml) was injected via the tail vein catheter over 4s. During the entire first phase the ventilator was turned off to simulate a breath hold and eliminate any respiratory motion in the liver.

In the second phase the ventilator was turned on (80 breaths per minute) and animals were scanned in cine mode for 1.2 seconds, every 10 seconds, up to a total of two minutes. After completion of the scan, images from the second phase were retrospectively gated to match the first phase images. Using the first phase images, a region of interest was drawn at the level of the diaphragm. From the 16 images in each of the second phase cine scans, the image that best matches the first phase images (acquired with breath hold) was manually selected based on image intensity. This proved to be a simple manual registration requiring only a few minutes to complete

per study. The smooth second phase of the portal venous and aortic time density curves demonstrate the aptitude of the retrospective gating method (Figure 3.1).

3.2.4 CT Perfusion Measurements / Data Analysis

CT images were analyzed using CT Perfusion software, which utilizes a dual input hybrid, compartment and distributed parameter, model. This model has been previously described and validated with microspheres in the rabbit liver [33]. As expressed in equation (1), a weighted sum of the aortic, $C_a(t)$, and portal venous, $C_{pv}(t)$, time density curves (TDC) were deconvolved against the liver parenchyma TDC, Q(t), in CT Perfusion (GE Healthcare) on a pixel-by-pixel basis to obtain the impulse residue function (IRF) [34,35] from which hepatic hemodynamic parameters are derived as explained below. The abdominal aorta was used as a surrogate for the hepatic artery due to its small size. Equation (2) defines the IRF, R(t)

$$Q(t) = F_T \cdot \left[\alpha C_a(t) + (1-\alpha) C_{pv}(t)\right] * R(t) \tag{1}$$

$$R(t) = \begin{cases} 0.0 & 0 \le t < T_0 \\ 1.0 & T_0 \le t \le T_0 + T_c \\ Ee^{-k(t-T_0-T_c)} & t > T_0 + T_c \end{cases} \tag{2}$$

F_T is the total hepatic blood flow. α is the fraction of total hepatic blood flow that is derived from the hepatic artery and thus, the hepatic arterial blood flow (F_a) is calculated as $\alpha \cdot F_T$. E is the extraction fraction of the contrast agent to the extra vascular space. k is the net back flow rate of the contrast from the extravascular space

to the intravascular space defined as $k= F_T E/Ve$, where Ve is the extra vascular volume. T_c is the mean transit time of the contrast agent from the arterial side to the venous side. T_0 is the appearance time of the contrast agent in the parenchyma relative to that of the aorta. Blood volume (V_b) is calculated as the product $F_T \cdot T_c$ via the Central Volume Principle. The permeability surface area product (PS) is calculated from the Crone relationship as $PS=-F_T \cdot \ln(1-E)$ [36].

Perfusion weighted (PW) maps were generated for each CT-Perfusion study by averaging the images in the first phase of each scan. In the PW maps the hepatic artery and portal vein branches appeared hyper-dense while the hepatic veins appeared hypo-dense. Using custom software (IDL v6.0; RSI Inc., CO, USA) a region of interest (ROI) was drawn on each PW map to encompass as much liver parenchyma as possible while avoiding large vessels. Measurements were obtained by applying the set of liver ROIs for each study to its respective functional maps (F_T, F_a, α, V_b, T_c, PS) generated by CT-Perfusion.

3.2.5 Histological Analysis

After the final CT examination, rats were sacrificed with sodium pentobarbital overdose. Livers were removed and fixed in 10% buffered formalin. Multiple liver lobes were collected and embedded in paraffin and 5μm thick slices were obtained for histological analysis. The slices were then stained with methyl blue and mounted on slides. The slides were digitized using an Aperio Scan Scope system (Aperio Technologies Inc., Vista, Ca, USA). Twelve images with an individual area of approximately $5mm^2$ were collected over multiple liver lobes of each rat. The ImageJ

software package [37] was used to measure percent positive area of stained collagen (PPAC). Thresholds were automatically determined using the maximum entropy method [38]. An example of a fibrotic liver stained with methyl blue is shown in Figure 3.3(A) and the resulting PPAC determined with Image J in Figure 3.3(B).

3.2.6 Statistical Analysis

Statistical analysis was performed using SPSS software (SPSS Inc., Chicago, IL, USA). A Mixed Model ANOVA was used as an omnibus test to identify significant differences between the control and CCl4 treated groups. Student t-tests with Bonferroni correction were used for post-hoc analysis of differences. To assess differences in PPAC between control rats and rats treated with CCl4 for 4, 6 and 8 weeks, independent unpaired t-tests for unequal variances were used. The Spearman correlation method was used to evaluate the relationship between the PPAC and α. A P-value <0.05 was regarded as statistically significant.

3.3 RESULTS

CT imaging and subsequent analysis was successfully performed in all animals at all time points. None of the rats suffered any obvious adverse effects from the CCl4 treatment nor did they develop any complication such as acities.

Liver samples in 3 animals (one treated with CCl4 for 6 week and 2 treated with CCL4 for 8 weeks) were not adequately fixed and thus, subsequent staining and digital image analysis could not be performed. For the other 22 rats (6 treated with

saline for 8 weeks and 6, 5, 8 treated with CCl4 for 4, 6, and 8 weeks respectively) PPAC was quickly and easily assessed. The mean PPAC for saline treated animals was 0.37%. The mean PPAC for animals treated with CCl4 was as follows; four weeks of treatment, 1.74%; 6 weeks of treatment, 2.31%; eight weeks of treatment, 2.20%. The PPAC of animals treated with CCl4 for 4, 6 and, 8 weeks were all significantly higher than controls ($P<0.002$). However weeks 4, 6 and, 8 were not significantly different from each other.

Figures 3.4 through 3.9 show measurements of F_T, F_a, α, V_b, T_c, and PS respectively over 8 weeks of treatment with either saline (control) or CCl4 (treated). The mixed model analysis showed that CCl4 treatment had a significant effect on F_T, F_a, α, and V_b but not T_c. PS showed a non-significant trend of increase with time in the treated group

Post hoc analysis using a two-tailed student t-test with Bonferroni correction showed significant differences in F_T, F_a, α, and V_b between control and treated animals. There was a significant difference in F_T between control and CCl4 treated animals at weeks 6 and 8, as well as between CCl4 treated animals at week 0 (baseline) and week 8. F_a showed a significant difference between treated and control animals at week 6. α showed a significant difference between control and CCl4 treated animals at weeks 4, 6 and, 8. α of CCl4 treated animals at weeks 4, 6, and 8 were also significantly higher from the baseline value. V_b for CCl4 treated animals at week 8 was significantly lower than baseline value and that of control animals at week 8.

A substantial correlation (r=.82 p<.00001) was observed between α and PPAC and is shown in Figure 3.10. All other perfusion parameters showed a low (r < 0.5) correlation with PPAC.

3.4 DISCUSSION

Digital image analysis was used in this study as a quantitative method for assessing liver fibrosis in excised liver sections. The common histopathological methods of assessing fibrosis has been the METAVIR staging system [8]. METAVIR was designed for the prognostic evaluation of biopsy from hepatitis C patients. Categorical staging methods place a larger emphasis on the patterns and structures present than the actual extent of fibrosis and are thus limited by their semi-quantitative nature as well as inter-observer variability. In contrast to this, digital image analysis uses a continuous variable and has implicitly high reproducibility and accuracy [39].

Of all the perfusion parameters only α showed a strong correlation (r=0.82 P<0.00001) with PPAC (Figure 3.10). The increase in α is caused by the hepatic arterial buffer response (HABR). As resistance to blood flow increases with collagen deposition as fibrosis progresses, portal blood flow has been shown to decrease. It is suspected that decreased washout of adenosine, a vasodilator, caused by decreased portal blood flow mediates an increase in hepatic arterial blood flow[31]. Thus, α, which is the ratio of F_a/F_T, increases with disease severity and may potentially be an excellent biomarker for liver fibrosis.

The CCl4 model of liver fibrosis used in this study is common and has been well explored [40]. Over the 8 weeks of treatment, liver fibrosis progressed from normal liver architecture to portal fibrosis with few septae and finally bridging fibrosis and cirrhosis (Figure 3.3). Only three of the treated animals developed cirrhosis. Although F_T and V_b did not correlate well with PPAC treated animals had significantly lower values than control animals after 8 weeks of treatment. While α seems to be a good biomarker for moderate fibrosis, F_T and V_b may be good biomarkers for predicting cirrhosis which was starting to develop in our model. Other perfusion studies of cirrhotic liver disease have found similar decreases in F_T and V_b[41,42]. Multiple biomarkers of different stages of liver disease may be useful for staging. Similar to serum marker algorithms, combinations of perfusion parameters could improve diagnostic performance and warrant further investigation.

The use of mechanical ventilation along with a paralytic agent allowed for a simulated breath hold in the animal. Along with a simple and fast manual registration technique almost all motion was eliminated from the cine scan. While this methodology cannot be used in patients, novel registration methods have the potential to substantially reduce breathing motion and noise respectively in clinical practice[43].

In our study the histological samples were not precisely matched to the location of perfusion analysis. Although liver disease is generally thought of as a diffuse disease, some heterogeneity has been shown to occur[11]. Thus, correlation of PPAC and perfusion parameters may have been improved if an exact match between the area analyzed at CT examination and histological samples could be obtained.

DCE-CT imaging carries with it the inherent risks of cancer induction/mortality and nephrotoxicity from ionizing radiation and iodinated contrast agents used in the study. Repeated imaging of the same location required for DCE imaging techniques can lead to high effective doses of typically 15-20 mSv in patients. However, newer iterative reconstruction techniques can reduce the effective dose by several fold. [44] [45]

DCE-MR offers a solution to radiation dose but has it's own drawbacks. Compared to DCE-CT, DCE-MR has a lower spatial resolution. Additionally, velocity-induced signal intensity changes in larger vessels has created difficulties in obtaining quantitative perfusion data with DCE-MR [46] [47].

For this study we used a commercially available dual input hybrid, compartment and distributed parameter, model (CT-Perfusion, GE Healthcare, Waukesha,WI, USA). Several different methods for the measurement of liver perfusion have previously been proposed [48] [29]. However, discrepancies between models used for perfusion analysis have been demonstrated [49]. Choice of method for the estimation of perfusion parameters must be assessed for each application. Models, and respective assumptions, must be applicable to the physiology of both the normal and disease states. Ideally, in-vivo validation of perfusion parameters against a non-model based gold standard would allow quantitative evaluation of various models. To this effect, microspheres have been used to validate hepatic arterial and portal venous blood flow in the liver [33] [29]. While these methods allow validation of blood flow other perfusion parameters such as blood (or distribution) volume, T_c and PS currently lack a strong reference standard for validation. Until all perfusion parameters can be

reliably validated, under normal and disease states, the utility of various models will depend largely on their diagnostic capability and availability.

In conclusion this study showed that perfusion parameters estimated with CT-Perfusion correlated with fibrosis content determined by digital image analysis. In particular, α, correlated very well ($r=0.82$ $P<0.00001$) with the progression of fibrosis and significant changes in F_T and V_b were observed when rats progressed to cirrhosis. These result show that CT-Perfusion is a useful method for quantifying hepatic fibrosis and subsequent progression to cirrhosis.

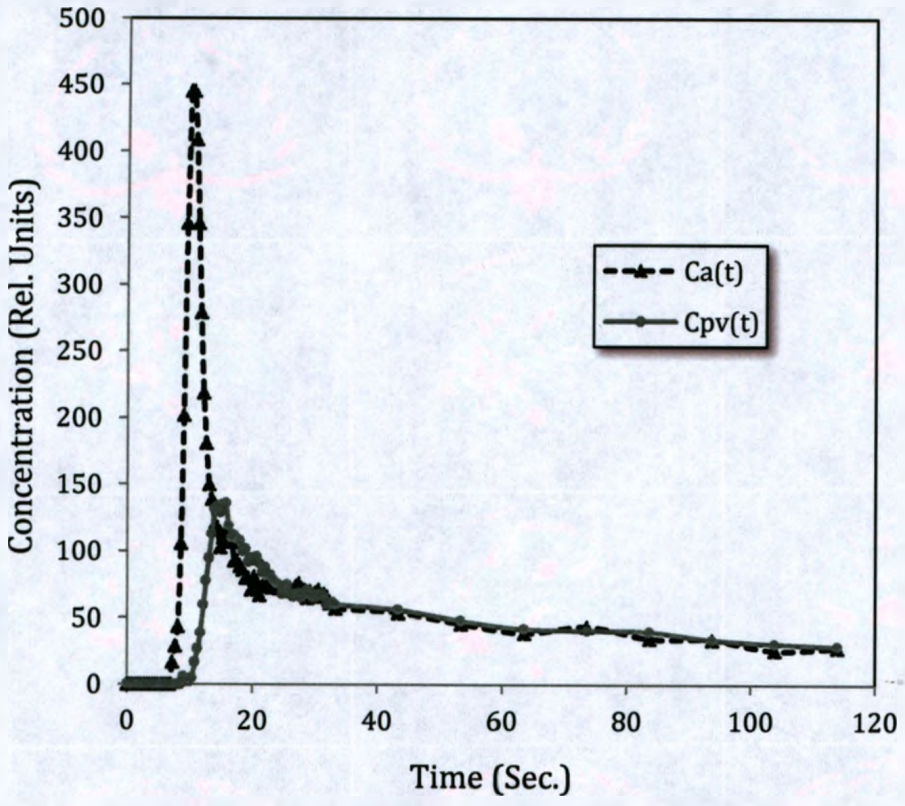

Figure 3.1 Concentration time curves from the abdominal aorta, Ca(t), and the portal vein, Cpv(t), acquired from actual CT data of a rat. The smooth nature of the second phase demonstrates the aptitude of the registration method used.

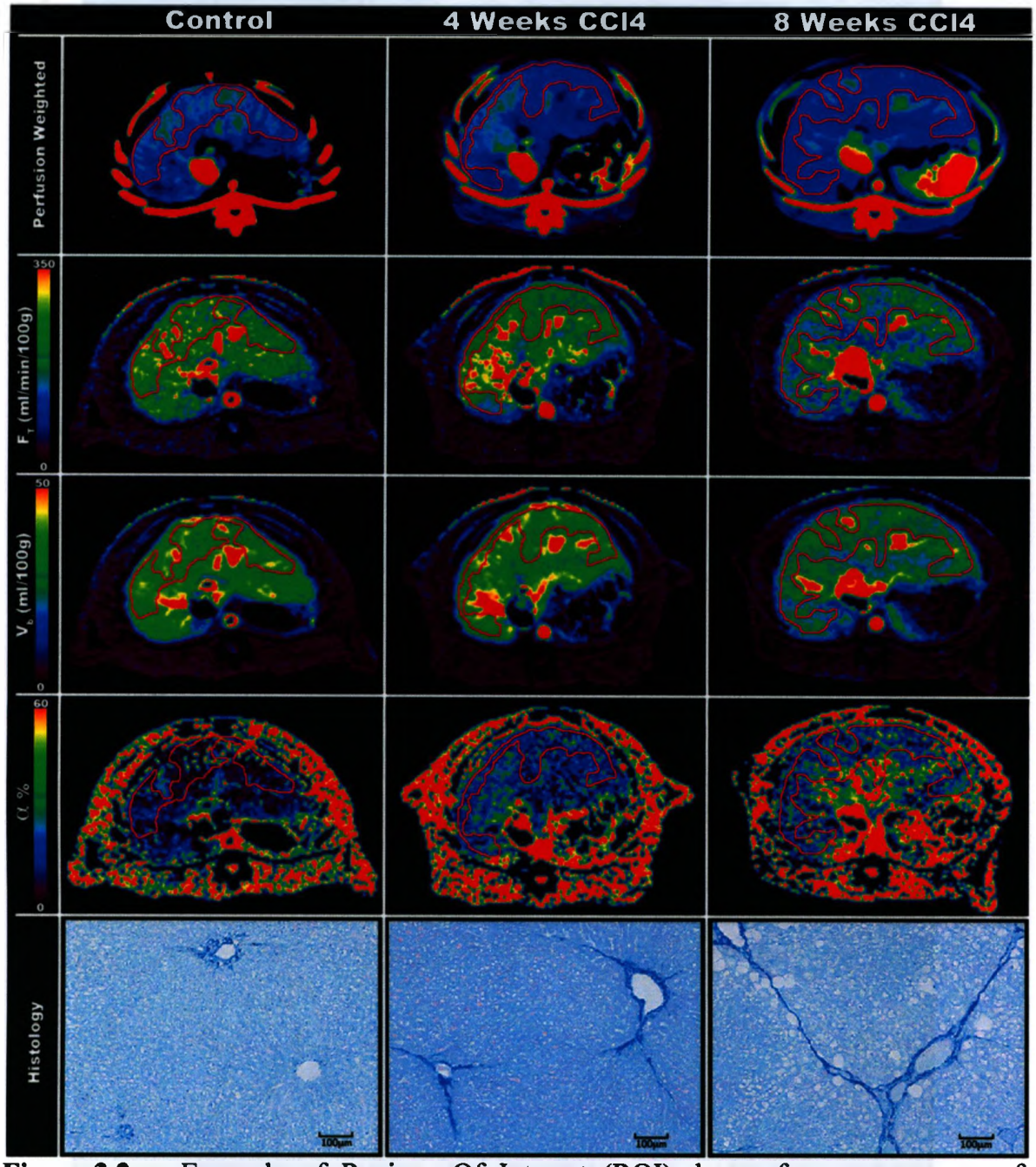

Figure 3.2 Example of Regions Of Interest (ROI) drawn for measurement of perfusion parameters. Care was taken to include as much liver parenchyma as possible while excluding large vessels. Histology was stained with methyl blue for collagen. Decreased hepatic blood flow (F_T) and blood volume (V_b) can been seen after 8 weeks of treatment. And increase in arterial fraction of blood flow (α) can be seen after only 4 weeks of treatment.

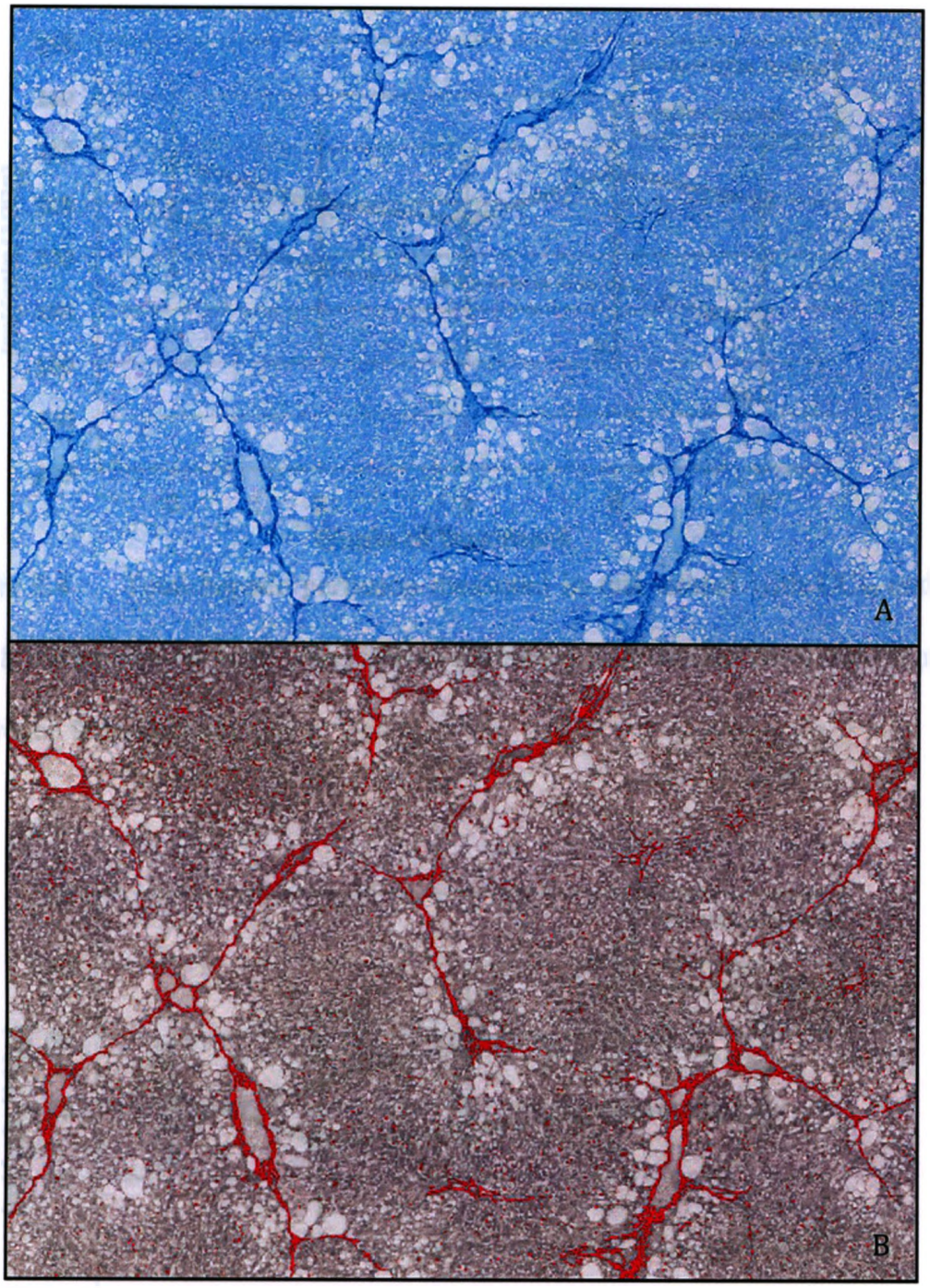

Figure 3.3 An example of quantification of liver fibrosis with digital image analysis. Sample image used for quantification (top) and 8-bit converted imaged for digital image analysis (bottom). Red area corresponds to the percent positive area of collagen (PPAC). In this example PPAC was 2.9% of the total area.

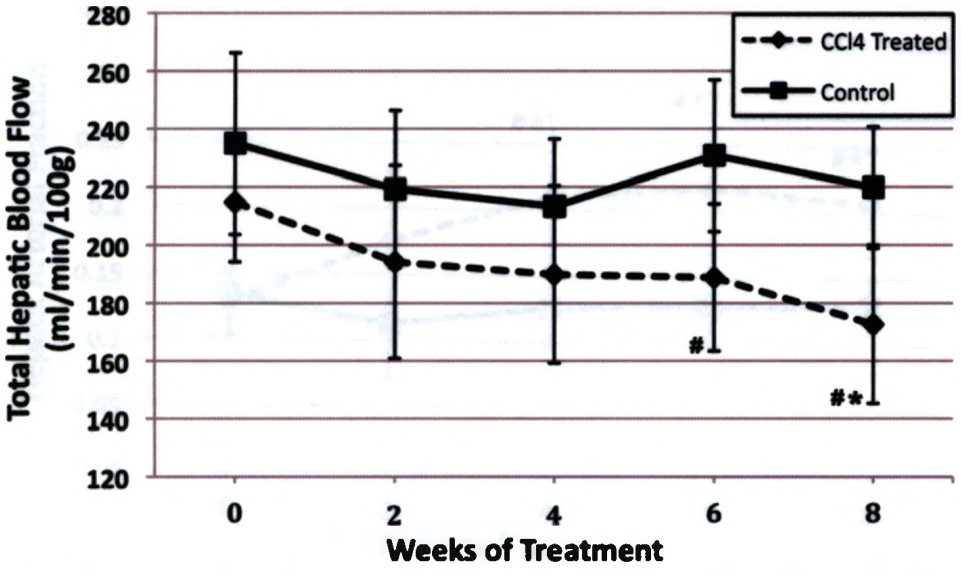

Figure 3.4 Total hepatic perfusion measured in rats treated with CCl_4 and saline over 8 weeks of treatment. (*significant difference from treated baseline; #significant difference from control)

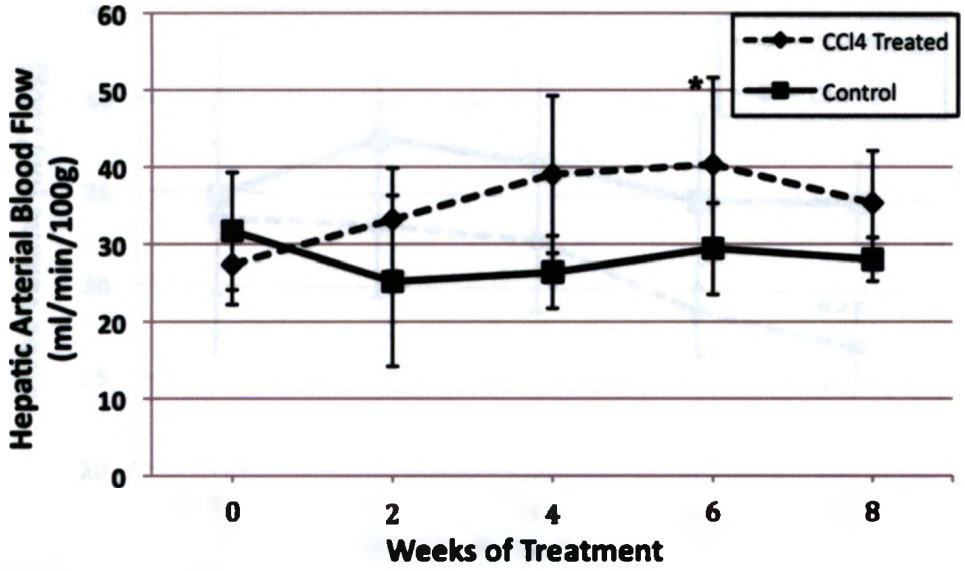

Figure 3.5 Hepatic arterial blood flow measured in rats treated with CCl_4 and saline over 8 weeks of treatment. (*significant different from treated baseline)

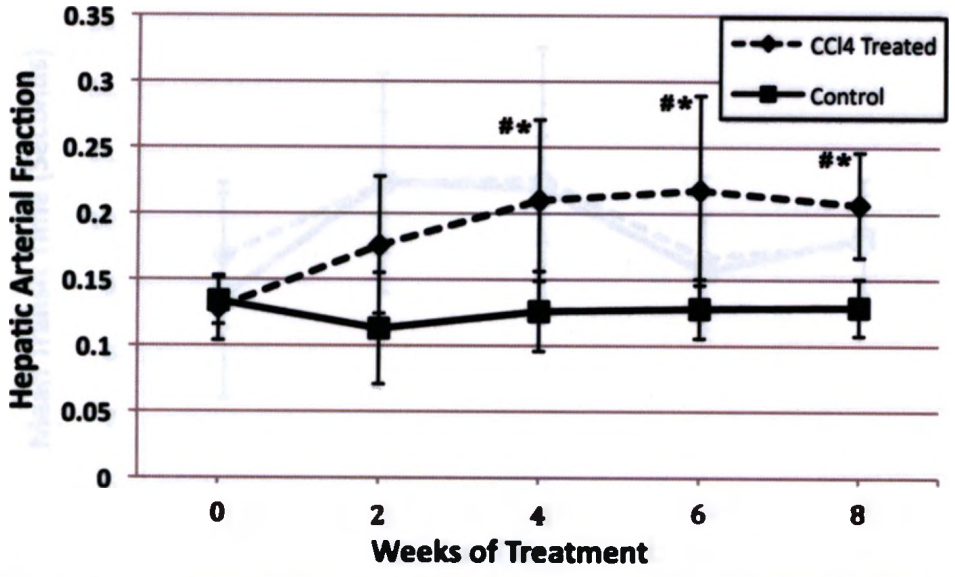

Figure 3.6 Hepatic arterial fraction of blood flow measured in rats treated with CCl_4 and saline over 8 weeks of treatment. (*significant difference from treated baseline; #significant difference from control)

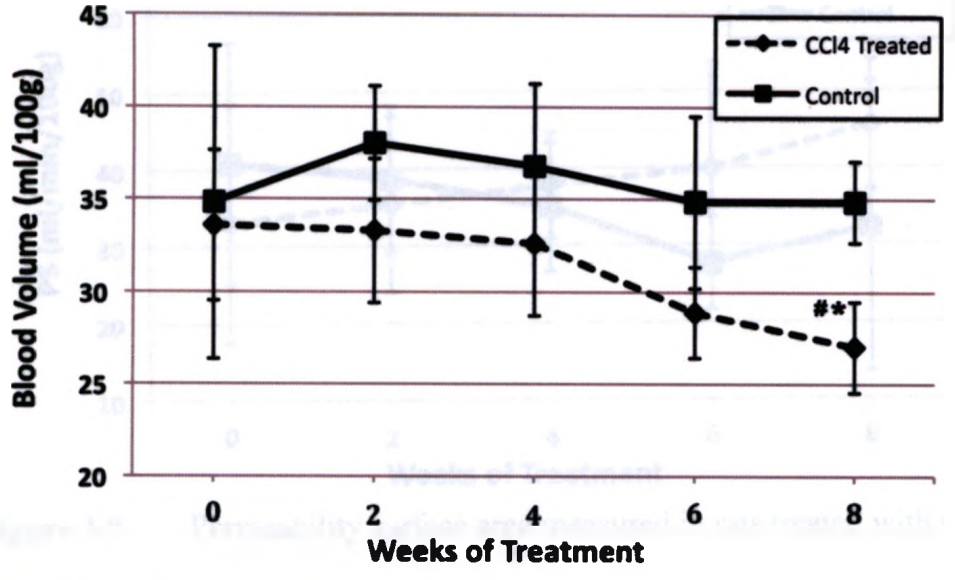

Figure 3.7 Blood volume measured in rats treated with CCl_4 and saline over 8 weeks of treatment. (*significant difference from treated baseline; #significant difference from control)

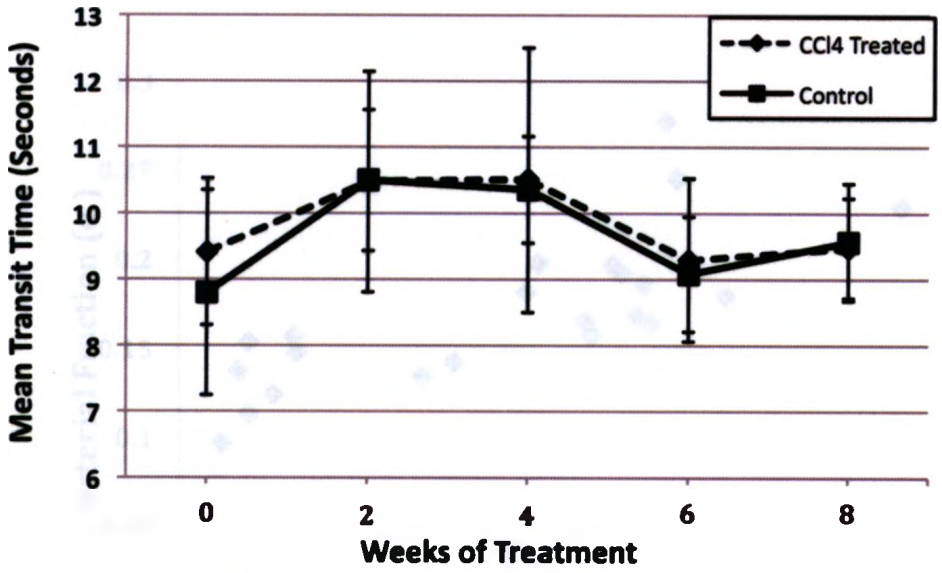

Figure 3.8 Mean vascular transit time measured in rats treated with CCl_4 and saline over 8 weeks of treatment.

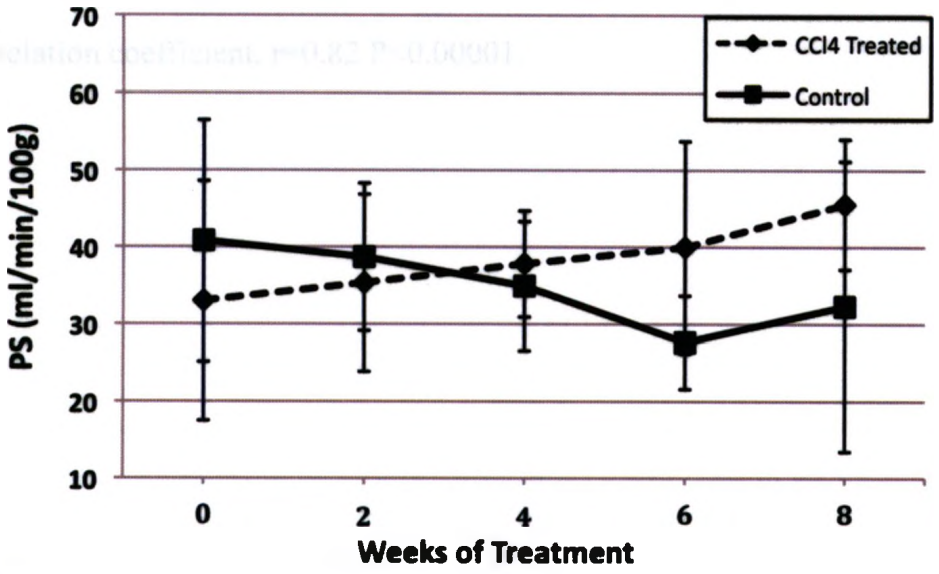

Figure 3.9 Permeability surface area measured in rats treated with CCl_4 and saline over 8 weeks of treatment.

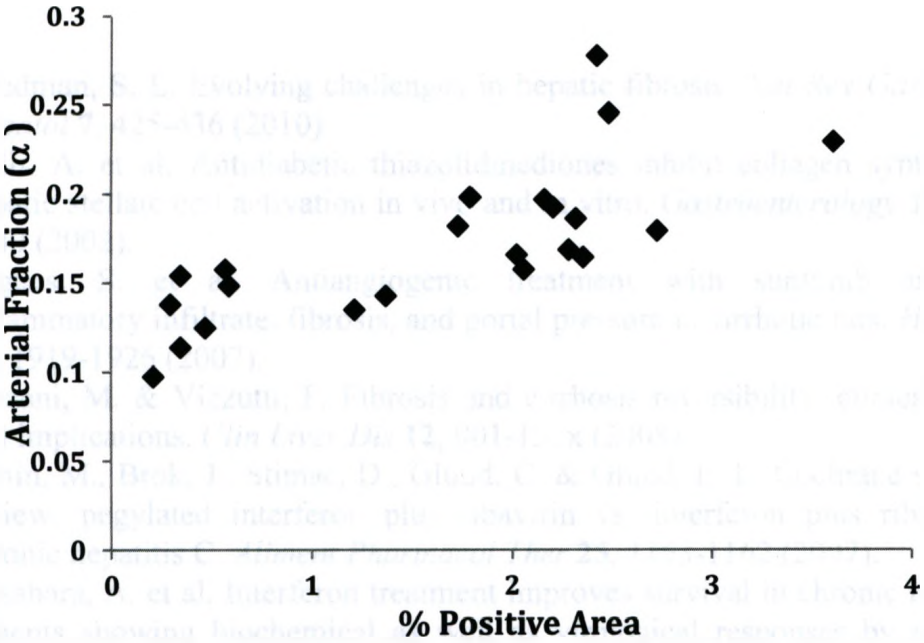

Figure 3.10 Correlation between hepatic arterial fraction and percent positive area of collagen (PPAC) from digital image analysis of liver specimens. Spearman correlation coefficient, r=0.82 P<0.00001.

3.5 REFRENCES

1. Friedman, S. L. Evolving challenges in hepatic fibrosis. *Nat Rev Gastroenterol Hepatol* **7**, 425-436 (2010).
2. Galli, A. et al. Antidiabetic thiazolidinediones inhibit collagen synthesis and hepatic stellate cell activation in vivo and in vitro. *Gastroenterology* **122**, 1924-1940 (2002).
3. Tugues, S. et al. Antiangiogenic treatment with sunitinib ameliorates inflammatory infiltrate, fibrosis, and portal pressure in cirrhotic rats. *Hepatology* **46**, 1919-1926 (2007).
4. Pinzani, M. & Vizzutti, F. Fibrosis and cirrhosis reversibility: clinical features and implications. *Clin Liver Dis* **12**, 901-13, x (2008).
5. Simin, M., Brok, J., Stimac, D., Gluud, C. & Gluud, L. L. Cochrane systematic review: pegylated interferon plus ribavirin vs. interferon plus ribavirin for chronic hepatitis C. *Aliment Pharmacol Ther* **25**, 1153-1162 (2007).
6. Kasahara, A. et al. Interferon treatment improves survival in chronic hepatitis C patients showing biochemical as well as virological responses by preventing liver-related death. *J Viral Hepat* **11**, 148-156 (2004).
7. Yoshida, H. et al. Interferon therapy prolonged life expectancy among chronic hepatitis C patients. *Gastroenterology* **123**, 483-491 (2002).
8. Bedossa, P. & Poynard, T. An algorithm for the grading of activity in chronic hepatitis C. The METAVIR Cooperative Study Group. *Hepatology* **24**, 289-293 (1996).
9. Strader, D. B., Wright, T., Thomas, D. L. & Seeff, L. B. Diagnosis, management, and treatment of hepatitis C. *Hepatology* **39**, 1147-1171 (2004).
10. Veldt, B. J. et al. Sustained virologic response and clinical outcomes in patients with chronic hepatitis C and advanced fibrosis. *Ann Intern Med* **147**, 677-684 (2007).
11. Bedossa, P., Dargere, D. & Paradis, V. Sampling variability of liver fibrosis in chronic hepatitis C. *Hepatology* **38**, 1449-1457 (2003).
12. Bravo, A. A., Sheth, S. G. & Chopra, S. Liver biopsy. *N Engl J Med* **344**, 495-500 (2001).
13. Halfon, P. et al. Accuracy of hyaluronic acid level for predicting liver fibrosis stages in patients with hepatitis C virus. *Comp Hepatol* **4**, 6 (2005).
14. Guechot, J. et al. Diagnostic accuracy of hyaluronan and type III procollagen amino-terminal peptide serum assays as markers of liver fibrosis in chronic viral hepatitis C evaluated by ROC curve analysis. *Clin Chem* **42**, 558-563 (1996).
15. Walsh, K. M., Fletcher, A., MacSween, R. N. & Morris, A. J. Basement membrane peptides as markers of liver disease in chronic hepatitis C. *J Hepatol* **32**, 325-330 (2000).
16. Wong, V. S. et al. Serum hyaluronic acid is a useful marker of liver fibrosis in chronic hepatitis C virus infection. *J Viral Hepat* **5**, 187-192 (1998).

17. Park, G. J., Lin, B. P., Ngu, M. C., Jones, D. B. & Katelaris, P. H. Aspartate aminotransferase: alanine aminotransferase ratio in chronic hepatitis C infection: is it a useful predictor of cirrhosis? *J Gastroenterol Hepatol* **15**, 386-390 (2000).
18. Poynard, T. et al. Meta-analyses of FibroTest diagnostic value in chronic liver disease. *BMC Gastroenterol* **7**, 40 (2007).
19. Taouli, B. et al. Diffusion-weighted MRI for quantification of liver fibrosis: preliminary experience. *AJR Am J Roentgenol* **189**, 799-806 (2007).
20. Lewin, M. et al. Diffusion-weighted magnetic resonance imaging for the assessment of fibrosis in chronic hepatitis C. *Hepatology* **46**, 658-665 (2007).
21. Fujimoto, K. et al. Evaluation of the mean and entropy of apparent diffusion coefficient values in chronic hepatitis C: correlation with pathologic fibrosis stage and inflammatory activity grade. *Radiology* **258**, 739-748 (2011).
22. Sporea, I., Sirli, R., Popescu, A. & Danila, M. Acoustic Radiation Force Impulse (ARFI)--a new modality for the evaluation of liver fibrosis. *Med Ultrason* **12**, 26-31 (2010).
23. Myers, R. P., Elkashab, M., Ma, M., Crotty, P. & Pomier-Layrargues, G. Transient elastography for the noninvasive assessment of liver fibrosis: a multicentre Canadian study. *Can J Gastroenterol* **24**, 661-670 (2010).
24. Huwart, L. & van Beers, B. E. MR elastography. *Gastroenterol Clin Biol* **32**, 68-72 (2008).
25. Asbach, P. et al. Viscoelasticity-based staging of hepatic fibrosis with multifrequency MR elastography. *Radiology* **257**, 80-86 (2010).
26. Salameh, N. et al. Hepatic viscoelastic parameters measured with MR elastography: correlations with quantitative analysis of liver fibrosis in the rat. *J Magn Reson Imaging* **26**, 956-962 (2007).
27. Ronot, M. et al. Liver fibrosis in chronic hepatitis C virus infection: differentiating minimal from intermediate fibrosis with perfusion CT. *Radiology* **256**, 135-142 (2010).
28. Miles, K. A., Hayball, M. P. & Dixon, A. K. Functional images of hepatic perfusion obtained with dynamic CT. *Radiology* **188**, 405-411 (1993).
29. Materne, R. et al. Non-invasive quantification of liver perfusion with dynamic computed tomography and a dual-input one-compartmental model. *Clin Sci (Lond)* **99**, 517-525 (2000).
30. Friedman, S. L. Hepatic fibrosis -- overview. *Toxicology* **254**, 120-129 (2008).
31. Richter, S., Mucke, I., Menger, M. D. & Vollmar, B. Impact of intrinsic blood flow regulation in cirrhosis: maintenance of hepatic arterial buffer response. *Am J Physiol Gastrointest Liver Physiol* **279**, G454-62 (2000).
32. Wasser, S. & Tan, C. E. Experimental models of hepatic fibrosis in the rat. *Ann Acad Med Singapore* **28**, 109-111 (1999).
33. Stewart, E. E., Chen, X., Hadway, J. & Lee, T. Y. Hepatic perfusion in a tumor model using DCE-CT: an accuracy and precision study. *Phys Med Biol* **53**, 4249-4267 (2008).
34. Lawrence, K. S. S. & Lee, T. Y. An adiabatic approximation to the tissue homogeneity model for water exchange in the brain: I. Theoretical derivation. *Journal of Cerebral Blood Flow & Metabolism* **18**, 1365-1377 (1998).

35. Lawrence, K. S. S. & Lee, T. Y. An adiabatic approximation to the tissue homogeneity model for water exchange in the brain: II. Experimental validation. *Journal of Cerebral Blood Flow & Metabolism* **18**, 1378-1385 (1998).
36. CRONE, C. THE PERMEABILITY OF CAPILLARIES IN VARIOUS ORGANS AS DETERMINED BY USE OF THE 'INDICATOR DIFFUSION' METHOD. *Acta Physiol Scand* **58**, 292-305 (1963).
37. Abramoff, M. D., Magelhaes, P. J. & Ram, S. J. Image processing with ImageJ, Biophoton. *Int* **11**, 36–42 (2004).
38. Kapur, J. N., Sahoo, P. K. & Wong, A. K. C. A new method for gray-level picture thresholding using the entropy of the histogram. *Computer vision, graphics, and image processing* **29**, 273-285 (1985).
39. Masseroli, M. et al. Automatic quantification of liver fibrosis: design and validation of a new image analysis method: comparison with semi-quantitative indexes of fibrosis. *J Hepatol* **32**, 453-464 (2000).
40. Constandinou, C., Henderson, N. & Iredale, J. P. Modeling liver fibrosis in rodents. *Methods Mol Med* **117**, 237-250 (2005).
41. Chen, M. L. et al. Assessment of the hepatic microvascular changes in liver cirrhosis by perfusion computed tomography. *World J Gastroenterol* **15**, 3532-3537 (2009).
42. Hagiwara, M. et al. Advanced Liver Fibrosis: Diagnosis with 3D Whole-Liver Perfusion MR Imaging—Initial Experience1. *Radiology* **246**, 926 (2008).
43. Hachama, M., Desolneux, A., Cuenod, C. A. & Richard, F. J. A classifying registration technique for the estimation of enhancement curves of DCE-CT scan sequences. *Med Image Anal* **14**, 185-194 (2010).
44. Yu, Z., Thibault, J. B., Bouman, C. A., Sauer, K. D. & Hsieh, J. Fast model-based X-ray CT reconstruction using spatially nonhomogeneous ICD optimization. *IEEE Trans Image Process* **20**, 161-175 (2011).
45. Cornfeld, D., Israel, G., Detroy, E., Bokhari, J. & Mojibian, H. Impact of Adaptive Statistical Iterative Reconstruction (ASIR) on Radiation Dose and Image Quality in Aortic Dissection Studies: A Qualitative and Quantitative Analysis. *AJR Am J Roentgenol* **196**, W336-40 (2011).
46. Goh, V. & Padhani, A. R. Imaging tumor angiogenesis: functional assessment using MDCT or MRI? *Abdominal imaging* **31**, 194-199 (2006).
47. Assumpcao, L., Choti, M., Pawlik, T. M., Gecshwind, J. F. & Kamel, I. R. Functional MR imaging as a new paradigm for image guidance. *Abdominal imaging* **34**, 675-685 (2009).
48. Blomley, M. J. et al. Liver perfusion studied with ultrafast CT. *J Comput Assist Tomogr* **19**, 424-433 (1995).
49. Kudo, K. et al. Differences in CT perfusion maps generated by different commercial software: quantitative analysis by using identical source data of acute stroke patients. *Radiology* **254**, 200-209 (2010).

CHAPTER 4

SUMMARY AND FUTURE WORKS

4.1 SUMMARY

The primary objective of this thesis was to evaluate the utility of dynamic contrast enhanced computed tomography (DCE-CT) imaging in conjunction with CT Perfusion (GE Healthcare) for the investigation of fibrotic liver disease. Monte Carlo simulations and sensitivity analysis were used to characterize the bias, variance and covariance of perfusion parameters calculated with CT Perfusion. DCE-CT scans were performed bi-weekly on rats treated with peritoneal injections of CCl_4 to induce liver fibrosis and, by eight weeks of treatment, cirrhosis. Sham injected (control) rats were similarly imaged for comparison. The perfusion parameters: total hepatic blood flow (F_T), hepatic arterial blood flow (F_a), blood volume (V_b), mean vascular transit time (T_c), hepatic arterial fraction of blood flow (α), and permeability surface area (PS), were then derived from the DCE-CT scans using CT Perfusion. As treatment progressed, CCl_4 treated rats showed significant changes in perfusion parameters. Histological samples stained with methyl blue were collected at various stages of treatment. From these stained samples liver fibrosis was quantified with digital image analysis and correlated to perfusion parameters. A strong correlation was found between fibrosis content and hepatic arterial fraction of blood flow (α).

The next sections summarize results obtained in each set of experiments completed in this thesis; followed by a discussion of the experimental and clinical

relevance of all major findings. Monte Carlo simulations demonstrated reasonable bias and variance in perfusion parameter estimates. In addition we were able to illustrate significant changes in F_T, V_b, F_a, and α as fibrosis progressed in a CCl_4 rat model. This demonstrates the ability of DCE-CT imaging with CT Perfusion to quantitatively assess changes associated with vascular changes known to occur during the development of cirrhosis[1 2 3]. The chapter concludes with a discussion on potential avenues of further research.

4.2 ERROR ANALYSIS OF HEPATIC PERFUSION PARAMETERS CALCULATED WITH CT PERFUSION

Chapter 2 presents the results of the sensitivity analysis of perfusion parameters estimated with CT Perfusion software. Results of the Monte Carlo simulations are presented for normal, mild, and severe stages of liver fibrosis. All sensitivity and Monte Carlo simulations were conducted using hepatic arterial and portal venous input functions obtained from actual DCE-CT studies on rats. Sensitivity analysis showed that F_T was the most sensitive parameter followed by α, k, E, T_c, and T_0 respectively. Subsequent calculation of the correlation matrix showed high correlation between F_T and T_c. Monte Carlo simulations showed that the accuracy of parameter estimation amongst all parameters tended to decrease with increasing noise.

T_0 and V_b showed little change in bias for both increasing noise and disease severity. Bias remained stable for T_c and F_T estimates for the mild and severe disease states but increased with noise for the normal disease state. The accuracy of

estimating T_0 and T_c increased with increasing disease severity.

An interesting observation was the effect of constraints imposed by CT Perfusion software on the parameter estimates. These constraints imposed a bias on the parameter estimates, as could be seen in the Monte Carlo simulations. Of particular note, the bias over varying disease levels was inconsistent for F_T, T_c, and PS. This inconsistent bias could affect the ability to measure changes in perfusion parameters as liver disease progresses. Other parameter estimates such as V_b and α were accurate and consistent among all levels of disease severity.

4.3 IN-VIVO MONITORING OF THE DEVELOPMENT AND PROGRESSION OF HEPATIC FIBROSIS IN A CCl_4 RAT MODEL WITH CT PERFUSION

Chapter 3 presents a study tracking changes in perfusion parameters in a CCl_4 rat model of liver fibrosis. Animals were randomized into control (n=6) and CCl_4 treated (n=9) groups. Dynamic contrast enhance computed tomography (DCE-CT) scans were performed on all animals at baseline and after 2, 4, 6, and 8 weeks of treatment. After 8 weeks of treatment all animals were euthanized and livers were removed and stained for fibrosis with methyl blue. To obtain histology samples at intermediate levels of progression two additional groups of rats were treated with CCl_4. The first group (n=5) received treatment for 4 weeks and the second group (n=5) received treatment for 6 weeks. DCE-CT scans were performed in these two shorter treatment groups at the same time points as the first, 8-week treatment, group,

animals were euthanized and livers were removed for histological analysis at the end of experiment.

The DCE-CT scans were analysed with CT Perfusion software and the perfusion parameters, F_T, F_a, V_b, T_c, α, and PS were measured. Mixed model analysis showed that CCl_4 treatment had a significant effect on F_T, F_a, α, and V_b but not Tc or PS. Post hoc analysis using a two-tailed student t-test with Bonferroni correction showed significant differences in F_T, F_a, α, and V_b between control and treated animals. Digital image analysis was used to measure percent positive area of stained collagen (PPAC). A substantial correlation ($r=.82$ $p<.00001$) was observed between α and PPAC. All other perfusion parameters showed a low ($r < 0.5$) correlation with PPAC. The strong correlation between α and PPAC suggests that α is a sensitive biomarker of fibrosis progression in the liver. CT-Perfusion proved to be an effective tool for tracking known vascular changes associated with the development of cirrhosis in an animal model.

4.4 EXPERIMENTAL AND CLINICAL RELEVENCE

The studies completed in this thesis have a number of implications experimentally. In the first study the variance, bias and correlation of perfusion parameters calculated with CT Perfusion were characterized for the analysis of liver disease. Results of this study are applicable to the interpretation of rat and possibly patient liver DCE-CT studies analyzed with CT Perfusion.

In the second study a CT imaging method for measuring changes in perfusion parameters in a CCl_4 rat model of liver fibrosis was developed. Because of the non-invasive nature of the imaging method, repeat measurements can be made in the same subject. Furthermore, the CT hardware and relevant software used are widely available. The ability of CT Perfusion to rapidly and accurately assess tissue hemodynamics makes the methodology developed in this thesis useful for investigating liver diseases involving vascular changes of the liver. Of particular note would be cancer and ischemia/reperfusion injury in pre-clinical models.

The methods used in this thesis could be readily advanced to clinical use. The DCE-CT scanning protocol used the combination of a paralytic and a ventilator, allowing for a simple registration method to reduce motion and noise in the data set. This methodology is impractical in the clinical setting however, registration techniques and iterative reconstruction methods currently under development [4 5] could sufficiently reduce noise to acceptable levels. Radiation dose would not be a barrier to clinical implementation. DCE-CT imaging results in an effective dose to the subject of 15-20 mSv which, is similar to current clinical three-phase liver scans[6].

4.5 FUTURE WORKS

The presented studies show the potential of using DCE-CT with CT Perfusion to longitudinally follow hemodynamic changes associated with the progression of fibrotic liver disease. With an increased understanding of the mechanisms of fibrosis,

new treatment options are becoming available [7]. Future studies could use the methods developed in this thesis to aid in the assessment of potential anti-fibrotic treatments.

CT Perfusion has also been effectively used to study cancers of the liver [8]. Since 80% of hepatocellular carcinoma (HCC) occur in a cirrhotic background [9] a cirrhosis/HCC model would be of particular interest. A Dimethylnitrosamine model is capable of producing fibrosis and cirrhosis in rats and eventually HCC [10]. The methods developed in this thesis would be ideal for studying such a model, as well as evaluating potential anti-angiogenic treatments on both the development of cirrhosis and HCC.

4.6 LIMITATIONS

There are a few limitations to these studies. Parameters used for simulation and sensitivity analysis were only appropriate for the study of rat liver. The results can not be applied to studies in humans or other animal models where hepatic perfusion parameters differ.

Histological samples were not precisely matched to the location of perfusion analysis. Although liver disease is generally thought of as a diffuse disease, some heterogeneity has been shown to occur [11]. Thus, correlation of PPAC and perfusion parameters may have been improved if an exact match between the area analyzed at CT examination and histological samples could be obtained.

Although the CCl_4 rat model of liver fibrosis is commonly used and well understood[12] it has no direct human counterpart. The changes in perfusion parameters noted in the CCl_4 model may differ in alternative models of liver disease.

4.7 CONCLUSIONS

The most significant conclusions of this thesis are listed below:

1) DCE-CT with CT Perfusion can track changes in hepatic hemodynamics associated with the development of fibrotic liver disease.
2) The hepatic arterial fraction of blood flow is strongly correlated with liver collagen content in a CCl_4 rat model of liver fibrosis.

4.8 REFRENCES

1. Richter, S., M√°cke, I., Menger, M. D. & Vollmar, B. Impact of intrinsic blood flow regulation in cirrhosis: maintenance of hepatic arterial buffer response. *American Journal of Physiology-Gastrointestinal and Liver Physiology* **279**, G454 (2000).
2. Van Beers, B. E. et al. Hepatic perfusion parameters in chronic liver disease: dynamic CT measurements correlated with disease severity. *American Journal of Roentgenology* **176**, 667 (2001).
3. Lee, J. S., Semela, D., Iredale, J. & Shah, V. H. Sinusoidal remodeling and angiogenesis: A new function for the liver,Äêspecific pericyte? *Hepatology* **45**, 817-825 (2007).
4. Yu, Z., Thibault, J. B., Bouman, C. A., Sauer, K. D. & Hsieh, J. Fast model-based X-ray CT reconstruction using spatially nonhomogeneous ICD optimization. *IEEE Trans Image Process* **20**, 161-175 (2011).
5. Hachama, M., Desolneux, A., Cuenod, C. A. & Richard, F. J. A classifying registration technique for the estimation of enhancement curves of DCE-CT scan sequences. *Med Image Anal* **14**, 185-194 (2010).
6. Pandharipande, P. V., Krinsky, G. A., Rusinek, H. & Lee, V. S. Perfusion imaging of the liver: current challenges and future goals. *Radiology* **234**, 661-673 (2005).
7. Friedman, S. L. Mechanisms of hepatic fibrogenesis. *Gastroenterology* **134**, 1655-1669 (2008).
8. Stewart, E. E., Chen, X., Hadway, J. & Lee, T. Y. Hepatic perfusion in a tumor model using DCE-CT: an accuracy and precision study. *Physics in Medicine and Biology* **53**, 4249 (2008).
9. Tsukuma, H. et al. Risk factors for hepatocellular carcinoma among patients with chronic liver disease. *New England journal of medicine* **328**, 1797-1801 (1993).
10. Magee, P. N. & Barnes, J. M. The production of malignant primary hepatic tumours in the rat by feeding dimethylnitrosamine. *British Journal of Cancer* **10**, 114 (1956).
11. Bedossa, P., Dargere, D. & Paradis, V. Sampling variability of liver fibrosis in chronic hepatitis C. *Hepatology* **38**, 1449-1457 (2003).
12. Tsukamoto, H., Matsuoka, M. & French, S. W. Experimental models of hepatic fibrosis: a review. *Seminars in liver disease* **10(1)**, 56 (1990).

APPENDIX A

Western

January 29, 2007

This is the Original Approval for this protocol
A Full Protocol submission will be required in 2011

Dear Dr. Lee:

Your Animal Use Protocol form entitled:
Perfusion and Lipid Imaging with a Liver Specific CT Contrast Agent to Detect Progression of Cirrhosis
Funding Agency CIHR - applied for

has been approved by the University Council on Animal Care. This approval is valid from **January 29, 2007** to **January 31, 2008.** The protocol number for this project is **#2007-025-01 and replaced #2005-051-07 (pilot).**

1. This number must be indicated when ordering animals for this project.
2. Animals for other projects may not be ordered under this number.
3. If no number appears please contact this office when grant approval is received.
   If the application for funding is not successful and you wish to proceed with the project, request that an internal scientific peer review be performed by the Animal Use Subcommittee office.
4. Purchases of animals other than through this system must be cleared through the ACVS office. Health certificates will be required.

ANIMALS APPROVED FOR 1 YR.

Species	Strain	Other Detail	Pain Level	Animal # Total for 1 Year
Rat	Sprague Dawley	~200 gm Male	C	16

STANDARD OPERATING PROCEDURES
Procedures in this protocol should be carried out according to the following SOPs. Please contact the Animal Use Subcommittee office (661-2111 ext. 86770) in case of difficulties or if you require copies.
SOP's are also available at http://www.uwo.ca/animal/acvs
310 Holding Period Post-Admission
320 Euthanasia
321 Criteria for Early Euthanasia/Rodents
330 Post-Operative Care/Rodent
343 Surgical Prep/Rodent/Recovery Surgery

REQUIREMENTS/COMMENTS
Please ensure that individual(s) performing procedures on live animals, as described in this protocol, are familiar with the contents of this document.

c.c. Approved Protocol
Approval Letter

Western

02.01.2010
***This is the 3rd Renewal of this protocol**
*A Full Protocol submission will be required in **01.31.2011**

Dear Dr. **Lee**

Your Animal Use Protocol form entitled:

Perfusion and lipid imaging with a liver specific CT contrast agent to detect progression of cirrhosis

has had its yearly renewal approved by the Animal Use Subcommittee.

This approval is valid from **02.01.2010 to 01.31.2011**

The protocol number for this project remains as **2007-028**

1. This number must be indicated when ordering animals for this project.
2. Animals for other projects may not be ordered under this number.
3. If no number appears please contact this office when grant approval is received.
   If the application for funding is not successful and you wish to proceed with the project, request that an internal scientific peer review be performed by the Animal Use Subcommittee office.
4. Purchases of animals other than through this system must be cleared through the ACVS office. Health certificates will be required.

REQUIREMENTS/COMMENTS
Please ensure that individual(s) performing procedures on live animals, as described in this protocol, are familiar with the contents of this document.
The holder of this *Animal Use Protocol* is responsible to ensure that all associated safety components (biosafety, radiation safety, general laboratory safety) comply with institutional safety standards and have received all necessary approvals. Please consult directly with your institutional safety officers.

c.c.